



Interplay of disorder and type of driving in disordered ferromagnetic systemsDjordje Spasojević  and Stefan Graovac *Faculty of Physics, University of Belgrade, P.O. Box 44, 11001 Belgrade, Serbia*Sanja Janičević *Faculty of Science, University of Kragujevac, P.O. Box 60, 34000 Kragujevac, Serbia* (Received 18 May 2022; revised 21 August 2022; accepted 19 September 2022; published 10 October 2022)

We investigate the effects of adiabatic, quasistatic, and finite-rate types of driving on the evolution of disordered three-dimensional ferromagnetic systems, studied within the frame of the nonequilibrium athermal random field Ising model. The effects were examined in all three domains of disorder (low, high, and transitional) for all types of driving, and in a wide range of driving rates for quasistatic and finite-rate driving, providing an extensive overview and comparison of the joint effects that the disorder, type of driving, and rate regime have on the system's behavior.

DOI: [10.1103/PhysRevE.106.044107](https://doi.org/10.1103/PhysRevE.106.044107)**I. INTRODUCTION**

Intermittent activity bursts are found as a share-ground in the response of various systems when they are exposed to external triggering. Such systems—including earthquakes [1,2], epidemics [3], financial stock markets [4], granular materials [5], crystal dislocations [6], disordered magnetic systems [7–10] and neuronal avalanches [11,12]—express diversity both in their origin and the size scale they extend to, comprising the range of more than ten decades [13]. Despite all the differences, what this broad class of systems has in common is the mechanism of complex evolution in the form of collective responses called avalanches, which come in all sizes and durations, distributed according to the power-law function of their parameters.

The relaxation dynamics in the above-mentioned complex systems can be influenced by many factors, one of which is the way in which they are driven, and this is the focus of this study. Typically, three different types of driving can be applied, namely adiabatic driving, quasistatic driving, and driving with a finite rate. Adiabatic driving is conducted under strictly controlled conditions, and it represents a kind of idealization that can easily be achieved in numerical simulations, but not in real experiments. In this type of driving, an avalanche is initiated by external triggering, which is absent during the avalanche propagation, and then applied again only to initiate the next one. The external triggering is also absent during the system response in the case of quasistatic driving, with the difference being that when applied it is realized in fixed increments of the triggering agent, which is possible both in real experiments and in simulations. Driving of the system in which the change of the external agent is conducted with a finite rate is even more realistic and comparable to experimental situations. Different ways of driving inflict differences in the system's behavior, one of the most obvious being the time/space profile of avalanche

evolution. In systems driven adiabatically, the propagation of a single avalanche at a time is ensured, while for the other two types of driving, simultaneous propagation of avalanches occurs. This propagation of avalanches can merge and spread as a joint system's activity, particularly for fast rates [14].

So far, the effects of different types of driving have been analyzed in a variety of papers. This holds for disordered ferromagnetic systems as well, in particular for those described by the random field Ising model (RFIM) [7] in its nonequilibrium (NE) zero-temperature (ZT) version [8,15,16]. In past studies of this model, much attention has been devoted to the behavior of adiabatically driven equilateral three-dimensional (3D) [16–18] and two-dimensional (2D) [19,20] systems, along with the dimensional crossover between these two [21]. After that, the influence of lattice topology was taken into consideration [22,23], together with the behavior of systems that are not equilateral [24–26]. Finite-rate driven systems have also been investigated, with a particular focus on the regime of high disorder [27–29], which enabled an analysis of the effects solely attributed to the driving rate [14,30,31]. In this paper, we put forward an extensive overview providing a comparison of the joint effects that the disorder, type of driving, and rate regime have within the frame of the NE-ZT-RFIM.

The paper is organized as follows: In Sec. II we introduce the model under study, the results obtained in numerical simulations are presented in Sec. III, and the Sec. IV is devoted to a discussion and conclusion. The paper ends with four Appendixes, providing more details on the effect of different choices of random field distribution on the response of the system, followed by a consideration of the system size effects, the flow of the pertinent effective critical parameters, and an explanation of the method for estimating the effective critical disorder.

II. MODEL

To model 3D equilateral disordered ferromagnetic systems, in this paper we use the nonequilibrium zero-temperature (i.e., athermal) version of the random field Ising model [8], which treats the set of Ising spins s_i (i.e., the spins having one of two possible values $+1$ or -1) located at the sites i of a cubic lattice. Each spin is exposed to the effects of three types of interactions: the ferromagnetic interaction with the nearest-neighboring spins, interaction with the external magnetic field, and the interaction with a random magnetic field that is quenched (i.e., unchanged during the evolution of the system) and allocated to each lattice site. Therefore, the Hamiltonian of the system, comprising all of these interactions, can be written in the form

$$\mathcal{H} = -J \sum_{(i,j)} s_i s_j - H \sum_i s_i - \sum_i h_i s_i, \quad (1)$$

where the summation in the first term, accounting for the ferromagnetic coupling with $J = 1$, runs over all nearest-neighboring spins. The values of the random field are mutually independent, uncorrelated, and, as in the majority of RFIM papers, taken from the Gaussian distribution

$$f_G(h) = \frac{e^{-h^2/2\sigma_G^2}}{\sigma_G \sqrt{2\pi}}, \quad (2)$$

whose standard deviation σ_G represents the disorder R of the system. For the effect of using other types of random field distributions, see Ref. [32] and Appendix A.

Provided a configuration of the quenched random magnetic field is chosen, Hamiltonian (1) enables finding the static equilibrium state of the zero-temperature RFIM system as the one having minimum energy at the given value of the external magnetic field H ; changes of such an equilibrium state, caused by variation of H , are studied in the *equilibrium* version of the model [32–39]. Contrary to the equilibrium version, in the nonequilibrium zero-temperature RFIM, the system evolves following an externally added local dynamical rule that is not stemming from Hamiltonian (1) but models the system's tendency to reduce its energy by adjusting spin orientation at each lattice site. The rule is based on the criterion for stability of spin orientation, according to which the spin s_i is *stable* at the current moment of time if it is aligned with the effective magnetic field

$$h_i^{\text{eff}} = J \sum_{j_i} s_{j_i} + H + h_i \quad (3)$$

at the spin's site i , so that $s_i h_i^{\text{eff}} > 0$; otherwise, if $s_i h_i^{\text{eff}} \leq 0$, the spin s_i is *unstable*.

Now, according to the local dynamical rule, each unstable spin will change its orientation at the following moment of (discrete) time, whereas the stable spins remain unchanged. As a consequence, the flipping of unstable spin will change the value of the effective magnetic field of all of its neighbors so that they might become unstable and change their orientation in the next moment, generating in this way a sort of collective cascade event of spin flipping called an *avalanche*. The avalanche lasts as long as there are unstable spins in the system, and it terminates when all spins become

stable. In this case, the whole system is in a stable state and remains in it until disturbed by some subsequent change in the external magnetic field. The stable state in question is not necessarily equilibrium but only one of the metastable states; in other words, in the nonequilibrium model, the system evolves through the metastable states tending to reach an energy minimum, unlike the equilibrium version in which the evolution, caused by variation of the external magnetic field, proceeds only through the equilibrium states.

The response signal of the NE-ZT-RFIM systems, given at each moment by the number of spins flipped at that moment, is not stationary in time. This is because the number of spins in the system is conserved, the energy cost for spin reversal (taken per unit of the external field change) depends on the system state, and lastly the response signal depends on how the system is driven. The only exception happens in the vicinity of the coercive field (more precisely, the effective external magnetic field defined in what follows) for the systems driven at a constant rate, where the number of spins flipped per unit of time is statistically at its maximum, so that the response signal, like in the Barkhausen noise experiments performed at a constant driving rate [9], becomes approximately statistically stationary in time.

The focus of this study is on the effects that different types of driving have on the NE-ZT-RFIM system's evolution. In the *adiabatic* driving, the system is driven by a one-step increase of the external magnetic field to the exact value that is causing the flipping of the least stable spin in the system, remaining unchanged during the ongoing avalanche. This type of driving leads to the propagation of a single avalanche at a time, therefore allowing for the statistical interpretation of the underlying events and avalanche parameters. In addition to adiabatic driving, we also studied the *quasistatic* type of driving, in which the magnetic field is incremented in fixed portions ΔH until the conditions are met for the unstable spin(s) to flip and consequently initiate one avalanche, or (occasionally) more avalanches separated in space. During the propagation of all avalanches triggered by each increment ΔH of the external field H , the current value of H is kept constant, and the incrementation of the field is continued after the end of the ongoing avalanche(s) until the initiation of the subsequent one(s). The occurrence of multiple avalanches, propagating during the same interval of time, constitutes the main difference between the adiabatic and quasistatic driving regimes, especially in the case of big increments ΔH . The third type of driving that we investigated here is the finite driving rate regime, in which the external magnetic field is increased at a constant rate $\Omega = \Delta H / \Delta t$ in *each time step*. For the sake of simplicity, in this paper we will use the same notation ΔH to indicate the field increment for both the quasistatic and finite driving rate regimes (because $\Delta t = 1$ is the increment of discrete time common for the considered driving regimes). The simultaneous propagation of spin avalanches becomes even more prominent in the case of finite driving, when temporal and/or spatial merging occurs shielding the contributions of individual avalanches and making it impossible to study the avalanches separately but only as a resulting superposition of multiple avalanche events occurring at the given time interval of the system's activity, as is argued in [14].

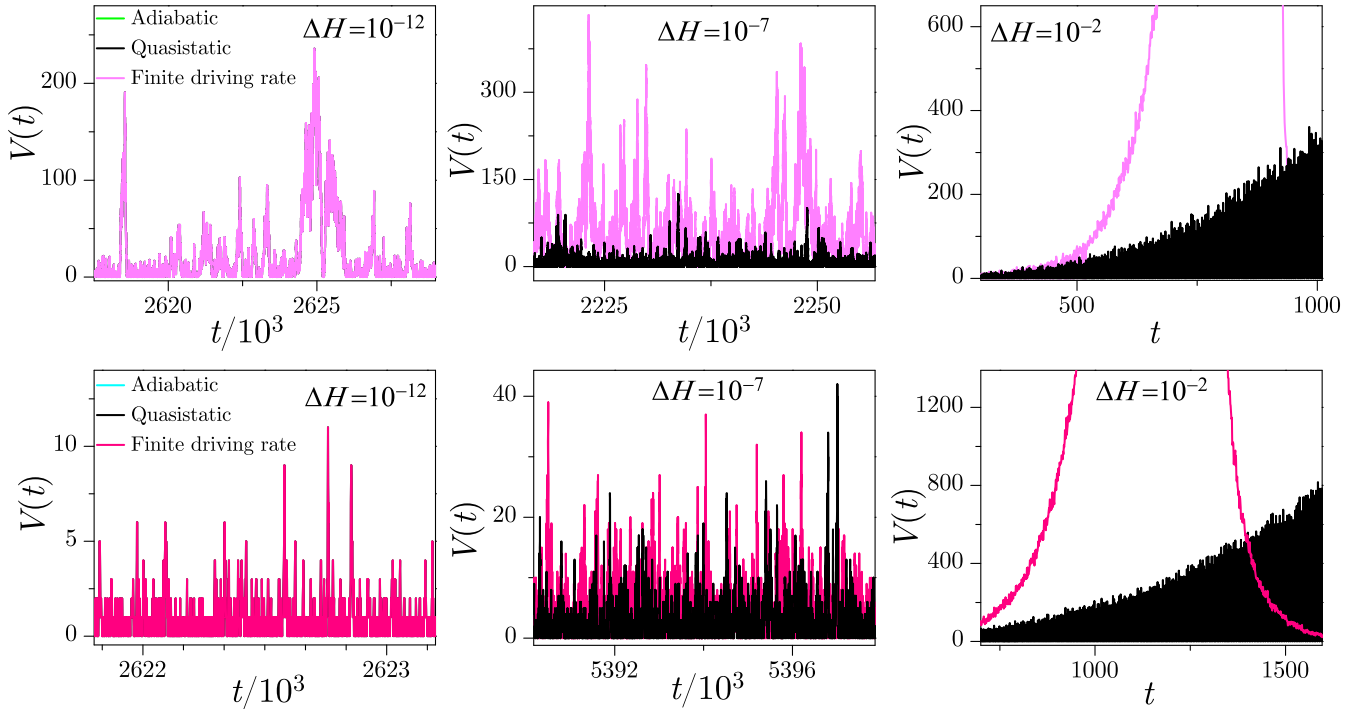


FIG. 1. Single-run signal samples for adiabatic, quasistatic, and finite-driving rate represented in the characteristic driving regimes of slow ($\Delta H = 10^{-12}$), intermediate ($\Delta H = 10^{-7}$), and fast driving ($\Delta H = 10^{-2}$). System size is $L = 256$, disorder $R = 2.35$ (top panels), and $R = 3.0$ (bottom panels). The signals overlap for all kinds of driving in the regime of adiabatic and very slow rates (panels from the first column). The differences begin to appear with the increase of driving rate, starting from the intermediate regime (middle column) and evolving to huge discrepancies present in the regime of fast rates (last column).

The starting point in our simulations is a stable configuration of all spins having sign -1 (pointing downwards) ensured by the very big and negative value of external magnetic field that dominates the overall effective magnetic field that each spin feels. The magnetic field is increased afterward for each type of driving accordingly, causing the spin-flipping avalanches. Flipping continues until all the spins change their orientation, ultimately reaching the new stability with all spins being aligned again with the same (upward) orientation $+1$, provided by the very big and positive value of magnetic field H .

III. RESULTS

In this paper, we have presented the results obtained in numerical simulations of the three-dimensional nonequilibrium athermal random field Ising model. We chose as a representative a system of linear size $L = 512$ that is big enough (containing 1.3×10^8 spins per lattice) and allows for the collection of a reliable amount of statistically averaged data in terms of the required simulations run-up time. For more details on the effect of the system size on its behavior, see Appendix B. Numerical simulations are based on the algorithm given in [20,40], adapted in a way to implement different types of driving employed.

The data presented in this paper are collected along the rising part of the hysteresis loop, comprising the change of the magnetic field in a range starting from a very big and negative value (e.g., -10), providing all spins are turned downwards, to a very big positive value (e.g., $+10$) when all the spins

have changed their orientation to align with the external field, i.e., up. The reported results are obtained in a wide range of driving rates, covering the regimes of slow, intermediate, and fast driving ($\Delta H = 10^{-12}$ – 10^{-2}), as well as for the disorders ranging from the subcritical, to the transient, to the supercritical domains ($R = 2.12$ – 4.0), for all characteristic types of driving. The boundary conditions employed are the periodic boundary conditions. In Fig. 1 we show the typical samples of the response signal $V(t)$ (equal to the number of spins flipped at the moment t) generated in a single run, i.e., one realization of a random magnetic field, for a given system and for all three types of driving. Here, the signals are obtained for the system size $L = 256$, with disorders $R = 2.35$ being slightly above and $R = 3.0$ being significantly above the effective critical disorder for a given system size. The effective critical disorder $R_c^{\text{eff}}(L)$ is a size-dependent nonuniversal parameter that tends in the thermodynamic limit to the critical disorder R_c [for more details on an estimation of $R_c^{\text{eff}}(L)$ values, see [17] and Appendix C]. One can see that the signals practically overlap for slow enough driving. The differences arise upon the increase in the driving rate, as is shown in the intermediate regime. The overall amplitudes, as well as their differences, are reduced with the increase of disorder (see the bottom panels), which is expected as the increase of disorder leads to the creation of smaller avalanches in the system. The biggest difference occurs for the fast driving rates, where the amplitudes of the signal generated with the finite driving are significantly higher (the full scope is not shown in the corresponding panels due to the scale difference) than for quasistatic driving.

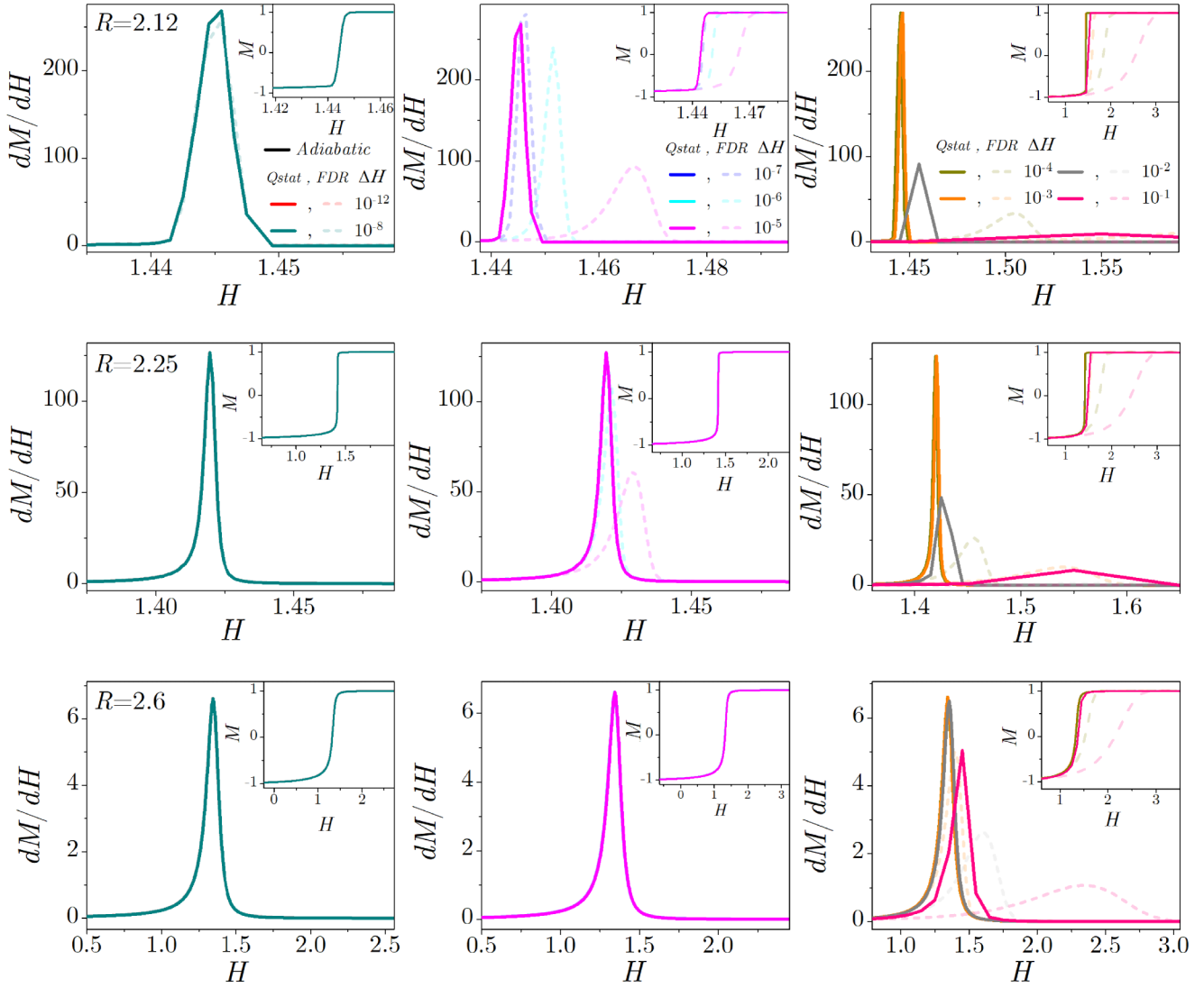


FIG. 2. Susceptibility and magnetization curves (shown in the main panels and in the insets) for systems with size $L = 512$ in slow, intermediate, and fast driving regimes for all types of driving and for disorders in domains $R < R_c$, $R \geq R_c^{\text{eff}}$, $R \gg R_c^{\text{eff}}$. Driving conditions for all panels in the same column are the same, and are indicated in the legend of the top panels. Disorder values, shown at the top of the leftmost panels, are the same for all panels in the same row. The data are averaged over 100 different realizations of random magnetic field.

A. Magnetizations

Magnetization of the system, $M = \frac{1}{N} \sum_{i=1}^N s_i$, and its derivative with respect to the magnetic field, i.e., magnetic susceptibility $\chi = \frac{dM}{dH}$, are typically the first quantities to look up in the field-driven ferromagnetic systems. The change in the shape of the magnetization curves is used as a qualitative guide to the underlying system's criticality. Namely, magnetization curves are smooth for disorders above the effective critical disorder $R_c^{\text{eff}}(L)$ for a given system size L , and they have a jump for disorders below it. These two cases are separated by the magnetization curve having the almost infinite slope at the effective critical value of external magnetic field $H_c^{\text{eff}}(L)$, where the pertinent susceptibility curve has the maximum.

In Fig. 2 we show the magnetizations (insets) and related susceptibilities (main panels) in the characteristic driving regimes (slow, intermediate, and fast) for the typical disorder

domains (subcritical, transient, and supercritical) for adiabatic, quasistatic, and finite rate driving. One can see that for the adiabatic and slow enough quasistatic and finite rate drivings, magnetization and susceptibility curves overlap regardless of the disorder domain to which they belong. With the increase in the driving rate, in the intermediate range, the differences start to emerge, being most pronounced for the disorders $R \leq R_c^{\text{eff}}(L)$, and slowly dissolving for disorders well above $R_c^{\text{eff}}(L)$. In the regime of fast driving rates, the discrepancies between the shapes of magnetizations and susceptibilities are even more expressed, persisting for the finite-rate driven systems even in the domains of high disorders. However, for the quasistatically driven systems, in the regime of very high disorders, $R \gg R_c^{\text{eff}}(L)$, magnetizations and susceptibilities become more and more indistinguishable. Ultimately, they become rate-independent, as is shown in Fig. 3, which resembles the size-independent behavior noticed

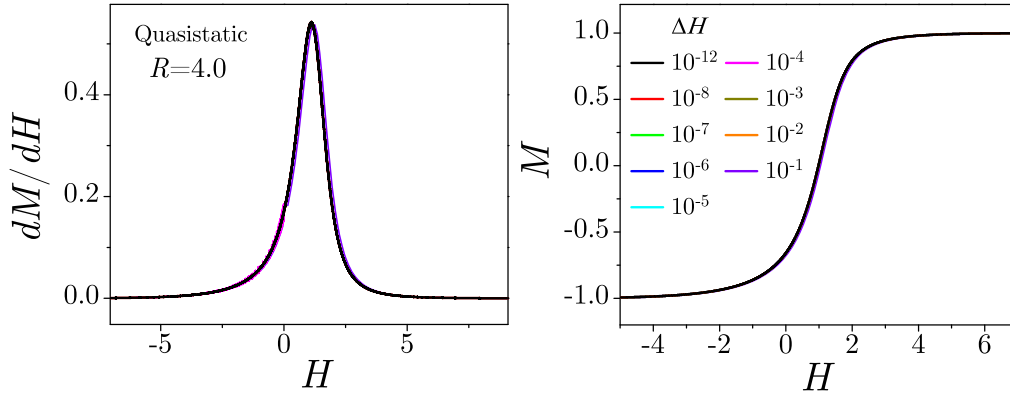


FIG. 3. Susceptibility and magnetization curves for the system of the same size $L = 512$ as in Fig. 2, driven quasistatically at the rates ΔH , shown in the legend of the right panel, in the domain of disorders $R \gg R_c^{\text{eff}}$; here $R = 4.0$. Presented curves overlap, marking the onset of rate independence.

for $R > R_c^{\text{eff}}(L)$ in the adiabatically driven systems [17]. In Fig. 4 we show the effective values of the critical magnetic field $H_c^{\text{eff}}(L)$ as a function of driving rate, estimated from the corresponding maxima of the susceptibility curves for the cases of quasistatic and finite driving. Qualitatively speaking, a similar dependence can be seen in both types of driving, and the flow of $H_c^{\text{eff}}(L)$ with ΔH retains its shape regardless of the value of R . Regarding the coercive field [i.e., the value of the external magnetic field corresponding to zero magnetization, and which is practically indistinguishable from the $H_c^{\text{eff}}(L)$ in our simulations], a similar rate dependence is experimentally observed on thin Fe films [41].

B. Distributions

Distributions of avalanche parameters, such as the size S and duration T , follow cutoff-terminated power laws characterized by the pertaining exponents, e.g., the exponent τ in the case of distributions $D(S) \sim S^{-\tau}$ of avalanche size S . These distributions, collected along the whole magnetization curve, are called the integrated distributions and encompass all types of avalanches generated in the system. A special role is played by the *spanning avalanches*, defined as the avalanches that span the system along at least one of the spatial dimensions

and thereby classified as 1D, 2D, and 3D according to the number of dimensions they span [42–44]. When the spanning avalanches are present, caused by a low enough value of disorder and/or by a high enough driving rate, they affect the shape of distribution altering the slope of its scaling region in the log-log plot, and consequently the value of the pertinent effective exponent. To examine the contribution from each type of avalanche (spanning and nonspanning), one has to distinguish and analyze their distributions separately.

Integrated size distributions in 3D systems in the presence of spanning avalanches contain contributions of nonspanning avalanches, and of some (or all) types of spanning avalanches [42–44]. In Fig. 5 we show several examples of the integrated avalanche size distributions for three characteristic values of disorder chosen as a representative of each disorder domain, covering a wide range of driving rates and types of driving. In the slow driving regime (first column of Fig. 5), the distributions almost overlap in all domains of disorder. With the increase in the rate, in the intermediate driving regime (middle column of Fig. 5), differences between the distributions driven quasistatically and with a finite driving rate become visible, becoming more and more apparent with the increase of disorder. Differences are most evident in the fast driving regime (last column of Fig. 5) where, besides the notable change in

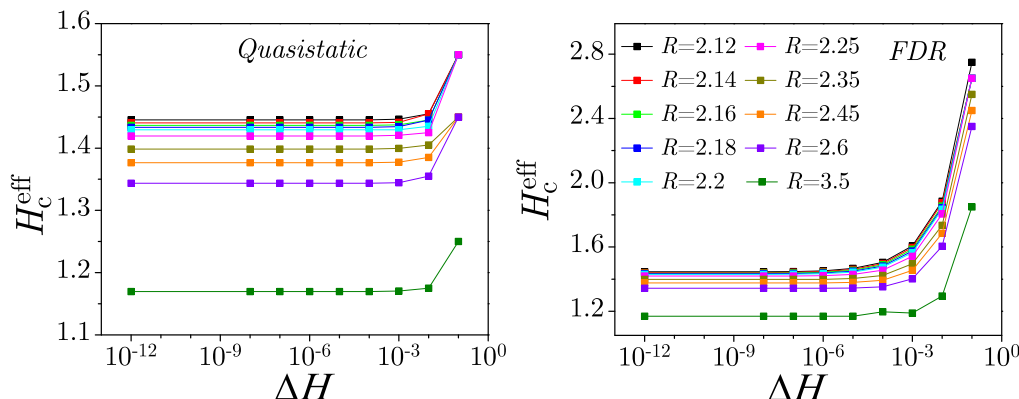


FIG. 4. The effective critical magnetic field H_c^{eff} in a wide range of driving rate ΔH for the quasistatic and finite driving of the system with the same size $L = 512$ as in Fig. 2, and in a wide range of disorders (see the legend of the right panel) used for both types of driving.

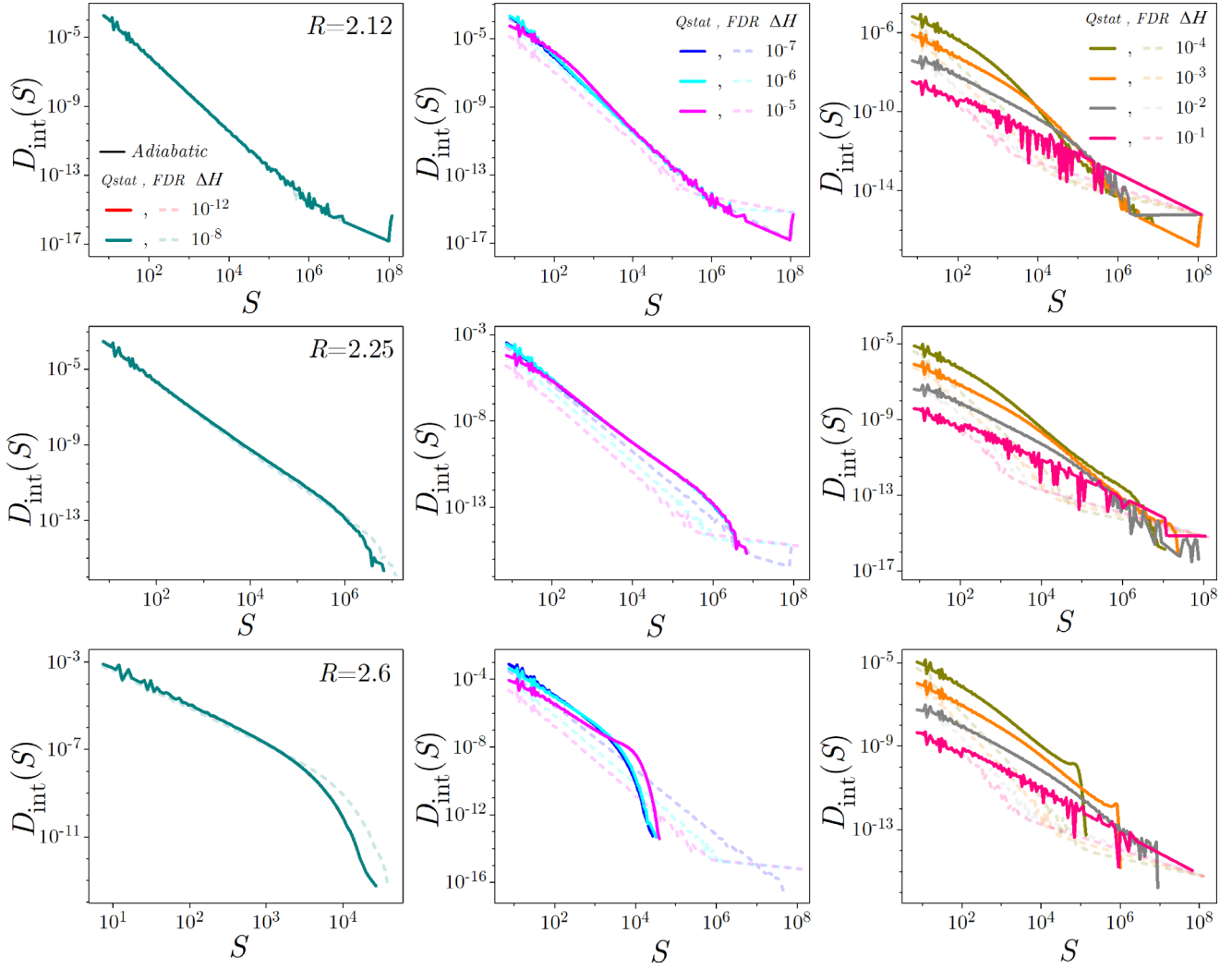


FIG. 5. Integrated avalanche size distributions for disorders $R < R_c$, $R \geq R_c^{\text{eff}}$, and $R \gg R_c^{\text{eff}}$ (presented in the rows, respectively) in the slow, intermediate, and fast driving regimes (presented in columns) for all types of driving (adiabatic, quasistatic, and finite rate) and for systems with the same size $L = 512$ as in Fig. 2.

the slopes of the distributions, characteristic bumps emerge at the end of the scaling regions marking the presence of the rate-induced spanning avalanches. To estimate the effective values of the rate-dependent size exponent τ_{eff} , we have performed the fitting of the integrated size distributions shown in Fig. 5 in the spirit of experimental data analysis. One commonly used analytic functional form for this purpose, illustrated in the case of size distribution, is the stretched exponential

$$D_{\text{mod}}^{(\text{se})}(S) = AS^{-\tau_{\text{eff}}} \exp[-(S/C)^c] \quad (4)$$

specified by τ_{eff} , A , C , and c as the fitting parameters. Such a model function is suitable for the description of the power laws ending with a cutoff by appropriate choice of the cutoff exponent c and parameter C playing the role of characteristic cutoff size.

We used this form of model function in fitting the integrated size distributions without spanning avalanches, e.g., for the distributions obtained for $R = 2.25$ and 2.6 in the range of slow rates.

On the other hand, the stretched exponential form ceases to be suitable for the description of distributions containing

bumps preceding the cutoff, which appear due to spanning avalanches that are present for disorders below $R_c^{\text{eff}}(L)$ in any driving regime, and for fast enough driving and disorders surpassing $R_c^{\text{eff}}(L)$ in both the quasistatic and finite driving rate regimes. One functional form, which gives the estimates of τ_{eff} less affected by the presence of a bump, is the functional form previously introduced in [45],

$$D_{\text{mod}}^{(\text{b})}(S) = AS^{-\tau_{\text{eff}}} \exp[(S/B)^b - (S/C)^c], \quad (5)$$

containing two additional parameters, namely the bump exponent b and the bump characteristic size B , reducing to a stretched exponential for $B = \infty$. Note, however, that although the proposed form (5) can be considered as adequate for a description of the distributions $D(S)$ collected in the slow and intermediate driving regimes in their full range, this does not hold anymore in the fast regime due to the advent of two scaling parts. For such distributions, the fitting procedure is applied only to the scaling part preceding the bump and cutoff (i.e., the initial distribution part is excluded), and therefore the estimated τ_{eff} values have significantly larger uncertainties.

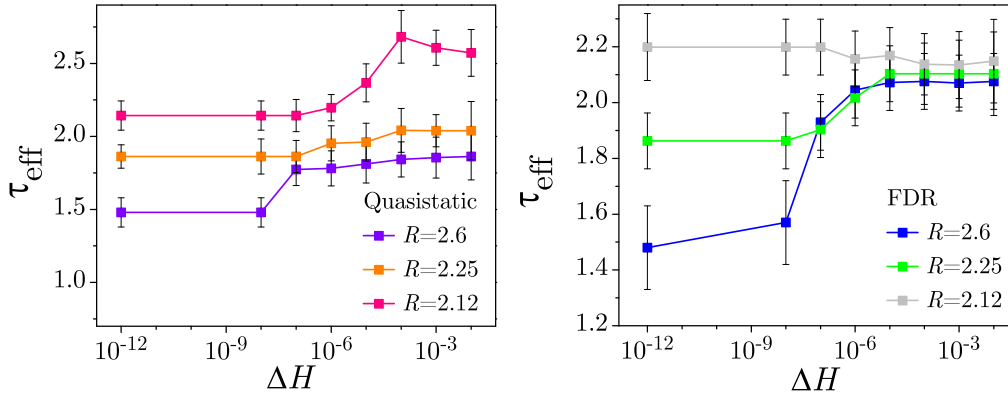


FIG. 6. Effective values of the rate-dependent effective size exponent τ_{eff} vs driving rate ΔH for the quasistatic (left panel) and finite-rate (right panel) driven systems estimated from the fits to the function (5). Error bars span the range of values estimated by fits.

In Fig. 6 we show the values of τ_{eff} versus the driving rate ΔH for the cases of quasistatic and finite driving, estimated from the fitting of the integrated size distributions shown in Fig. 5. Exponents for both types of driving, qualitatively speaking, show similar trends to the driving rate, remaining almost constant for slow enough rates, followed by the increase with the rate in the intermediate regime, regardless of the disorder domain. Reaching the regime of fast rates, exponent values saturate and remain approximately stable and constant. This flow of the effective values of exponent τ_{eff} with the driving rate ΔH is in agreement with the previously reported results addressing the case of highly disordered systems driven with a finite driving rate [30]. What can also be seen is that the overall variation of the exponent values is bigger for the quasistatic driving, while the range within which the exponents change in the case of finite driving is more narrow.

Figure 7 shows the integrated size distributions of non-spanning avalanches extracted from the integrated size distributions of all avalanches (presented in Fig. 5) by removing the contribution of spanning avalanches. It can be seen that these distributions overlap for all system parameters in the regime of slow driving regardless of the value of disorder and the type of driving, similarly to the integrated ones. With the increase in the rate, the distributions obtained from systems driven with a finite rate start to deviate from those that are quasistatically driven, even in the intermediate regime of rates, while for the fast rates the differences become even more expressed due to the onset of rate-induced spanning avalanches, which consequently influences the distributions of nonspanning avalanches as well. The characteristic sags, occurring close to the cutoff area, are present here for all values of disorder of the system both in the intermediate and fast driving regimes. These sags are attributed to the onset of spanning avalanches in the process of merging the nonspanning ones and were previously noticed for high disorders in [30].

In Figs. 8 and 9 we show the distributions of 1D, 2D, and 3D spanning avalanches, $D_{1D}(S)$, $D_{2D}(S)$, and $D_{3D}(S)$, for quasistatic and finite-rate driving, respectively, for some characteristic values of disorder. We can see that in the domain of very low disorder, the contribution from spanning avalanches due to the disorder dominates. With the increase in the driving rate and disorder, a second peak starts to emerge

on the right side of the distributions, marking the occurrence of rate-induced spanning. A further increase in the rate in the domain of very high disorder leads to the predomination of solely rate-induced spanning avalanches, blending the distributions to single-peaked again. In the insets of the main panels, we show the numbers of spanning avalanches per run as a function of driving rate for different disorders.

C. Correlations

In the adiabatic driving regime, the correlations at disorder R in the equilateral RFIM systems of size L are quantified by the avalanche correlation function $G_{R,L}(x; H)$ measuring a non-normalized probability of flipping a spin at a distance x ($x \geq 1$) from the initial spin of the ongoing avalanche propagating at the external field H . More precisely, $G_{R,L}(x; H)$ is calculated from the number $N_{R,L}(x; H)$ of the above-described spin flipping divided by the number of spins at a distance x from the initial spin and by the number of simulations. Near the critical point and for large distances x , the foregoing basic type of avalanche correlation function scales as

$$G_{R,L}(x; H) = \frac{1}{x^{d-2+\eta}} \mathcal{G}_{\pm}(x/\xi(R, H, L)), \quad (6)$$

and for compatibility with its usage in past RFIM studies (see, e.g., [8,17], as well as the references quoted therein) it is adopted in this paper as a starting point for further analysis of correlations. In (6), d is the dimension of the system, η is the exponent called the anomalous dimension, while \mathcal{G}_+ and \mathcal{G}_- are the universal scaling functions for disorders $R > R_c$ and $R < R_c$, both being functions of the single argument $x/\xi(R, H, L)$, i.e., distance x scaled by the correlation length $\xi(R, H, L)$. Being non-normalized, $G_{R,L}(x; H)$ depends on disorder R and surpasses the value 1 for small x ; see, e.g., the top panel of Fig. 18 in [8] and Fig. 15 in [17]. Note that the latter would not be the case if instead by the number of simulations, the number of spin flipping $N_{R,L}(x; H)$ was normalized by, e.g., the total number of avalanches, which would, however, violate the scaling (6).

In what follows, we will concentrate on the conceptually important integrated avalanche correlation function $G_{R,L}^{\text{int}}(x)$, which takes into account all avalanches along the entire rising part of the magnetization curve and is therefore

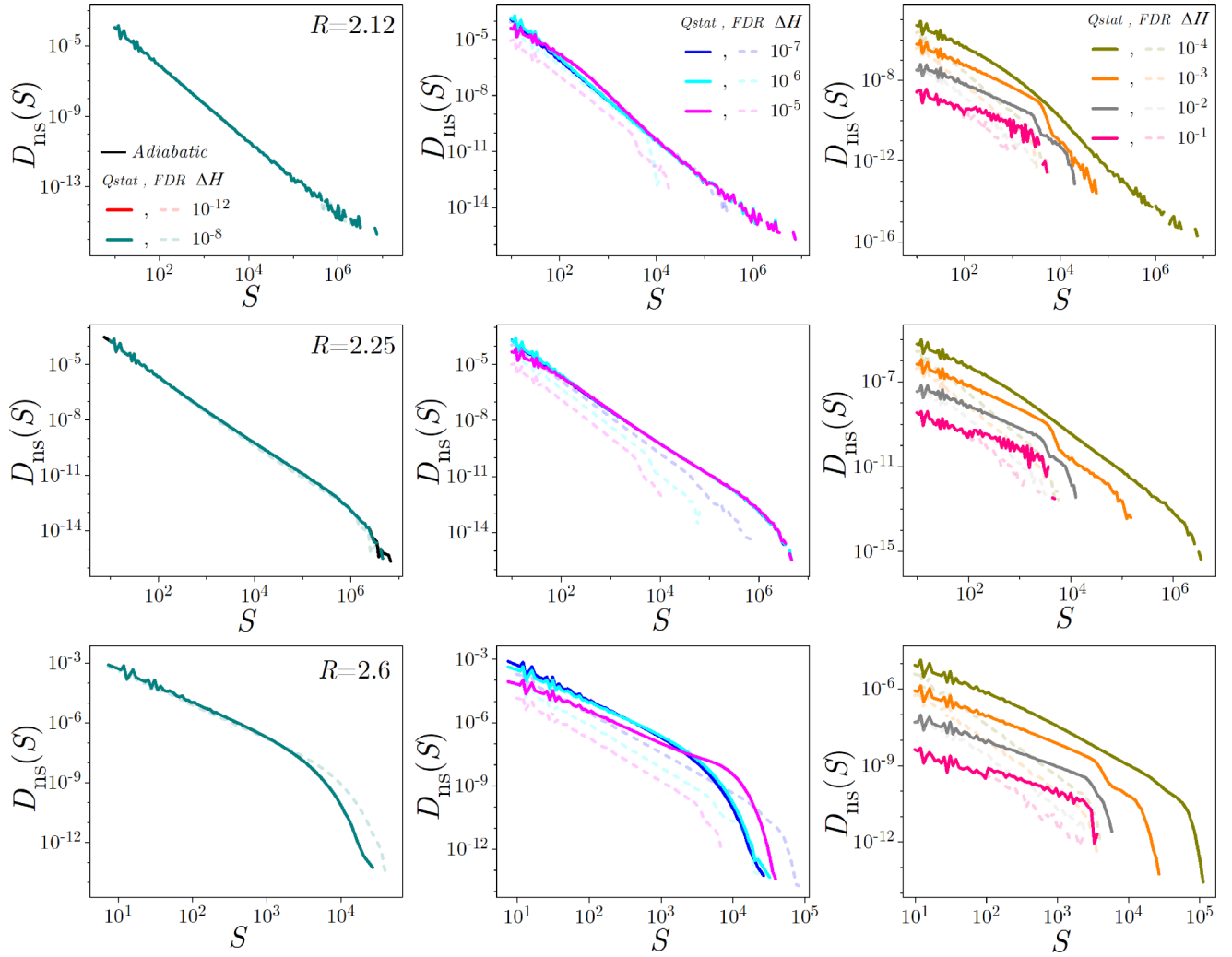


FIG. 7. Integrated nonspanning avalanche size distributions for the system with the same size $L = 512$ as in Fig. 2, and for disorders $R < R_c$, $R \geq R_c^{\text{eff}}$, and $R \gg R_c^{\text{eff}}$ (presented in the rows, respectively) in slow, intermediate, and fast driving regime (presented in columns) for all types of driving (adiabatic, quasistatic, and finite rate) with the driving rates from the legends in the top panels.

computationally far more efficient than $G_{R,L}(x; H)$ calculated only for the avalanches triggered within a narrow window of external field around its center H . Provided the system size L and reduced disorder $r = (R - R_c)/R$ satisfy the $rL^{1/\nu} = \text{const}$ condition, $G_{R,L}^{\text{int}}(x)$ scales as

$$G_{R,L}(x) = \frac{1}{x^{d+\beta/\nu}} \bar{G}_{\pm}(x|r|^{\nu}, 1/L|r|^{\nu}), \quad (7)$$

where \bar{G}_{\pm} are the universal scaling functions for the integrated avalanche correlation function $G_{R,L}^{\text{int}}(x)$, and β and ν are the standard RFIM exponents [17]. Already for moderately big L 's (say $L \geq 512$) and above critical disorder, $G_{R,L}^{\text{int}}(x)$ becomes practically indistinguishable from its thermodynamic limit $G_R^{\text{int}}(x) = \lim_{L \rightarrow \infty} G_{R,L}^{\text{int}}(x)$, see [17], and therefore regardless of the finite-size scaling tuning condition $rL^{1/\nu} = \text{const}$, satisfies the scaling

$$G_R(x) = \frac{1}{x^{d+\beta/\nu}} \bar{G}_{\pm}(x|r|^{\nu}), \quad (8)$$

introduced for $G_R(x)$ in [46].

In contrast with adiabatically driven systems where the avalanches propagate one at a time, in systems driven quasistatically and with a finite rate, multiple avalanches can propagate at the same time, which could lead to their spatial merging as well, which becomes even more prominent as the rate increases. The separation into individual contributions of single avalanches is not possible anymore, so the concept of an activity event as the joined superposition of a system's activity has been introduced in [14] for systems driven at finite rates along with the integrated activity correlation function $G_{\text{int}}^{\text{ae}}(x; R, \Omega, L)$. This function accounts for all activity events a probability per spin that the first spin flipping will result in the flipping of spins that are at a distance x within the same activity event. The same quantity can be introduced also in the quasistatic case because of the presence of the activity events in this driving regime. So, in this paper we consider the integrated triggered activity correlation functions $G_{\text{int}}^{\text{ta}}(x; R, \Omega, L) = L^3 G_{\text{int}}^{\text{ae}}(x; R, \Omega, L)$ which in the fast (enough) driving regime exhibit the plateau induced by the occurrence of spanning avalanches in the system.

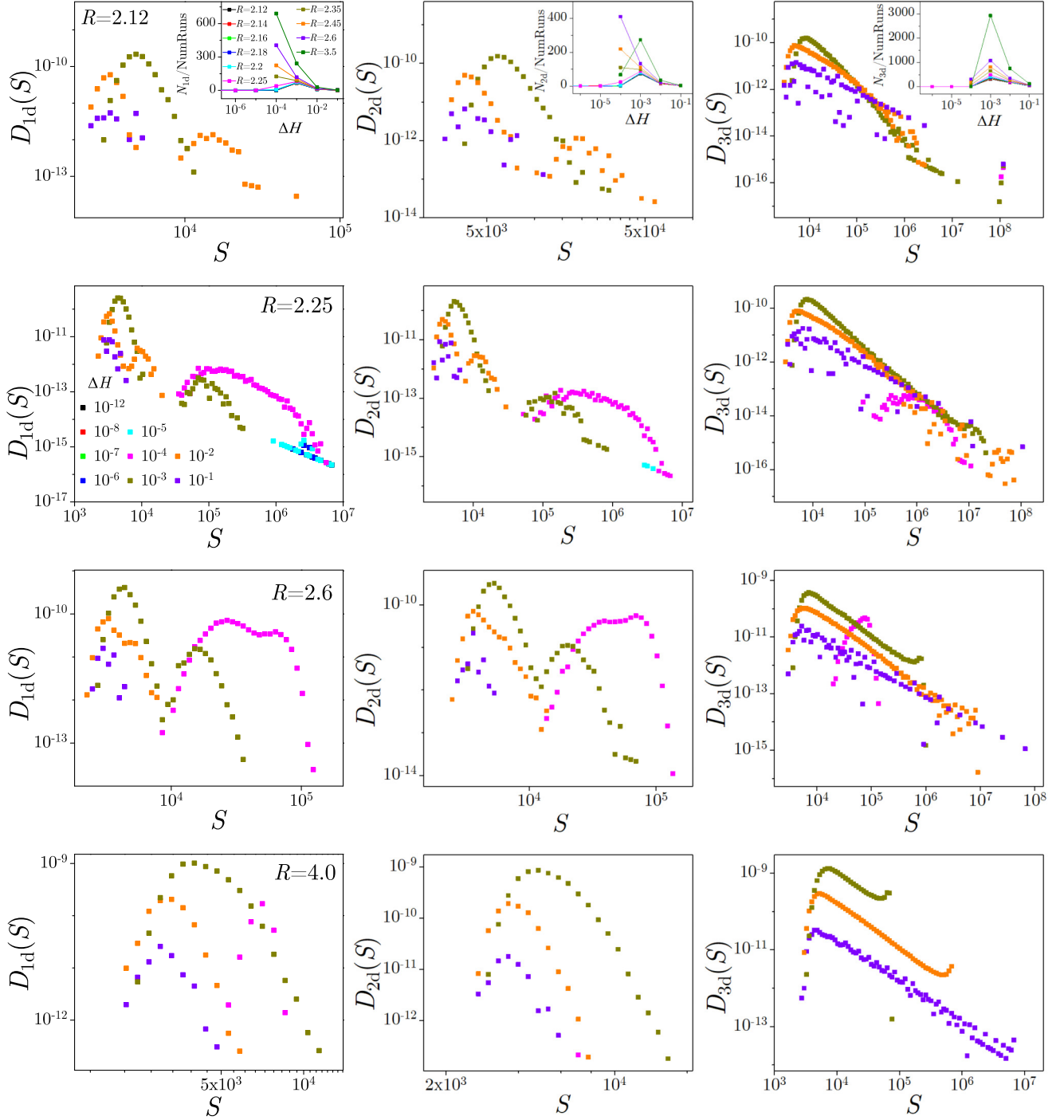


FIG. 8. Integrated size distributions of different types of spanning avalanches, $D_{1D}(S)$, $D_{2D}(S)$, and $D_{3D}(S)$, for disorders $R < R_c$, $R = R_c^{\text{eff}}$, $R > R_c^{\text{eff}}$, and $R \gg R_c^{\text{eff}}$ (shown in rows, respectively), in a wide range of driving rates of quasistatic driving. Insets show the number of particular types of spanning avalanches per single run vs the driving rate. The legend shown in the left panel in the second row applies to all main panels in this figure, while the legend in the inset of the left-top panel is valid for all insets presented in the first row.

In Fig. 10 we show the integrated triggered activity correlation functions covering a wide range of disorders, driving rates, and for all three types of driving. We see that the characteristic plateaus are present for disorders below the critical disorder, marking the onset of spanning avalanches regardless of the system's driving rate. For disorders that are close to

the effective critical disorder (middle row in Fig. 10), we see that for slow driving the plateau is absent, as are the spanning avalanches, mimicking the adiabatic case. With the increase in the rate, the plateau starts to emerge even in the intermediate regime of driving rates for the case of finite driving, being more sensitive to the increase in the rate, while the

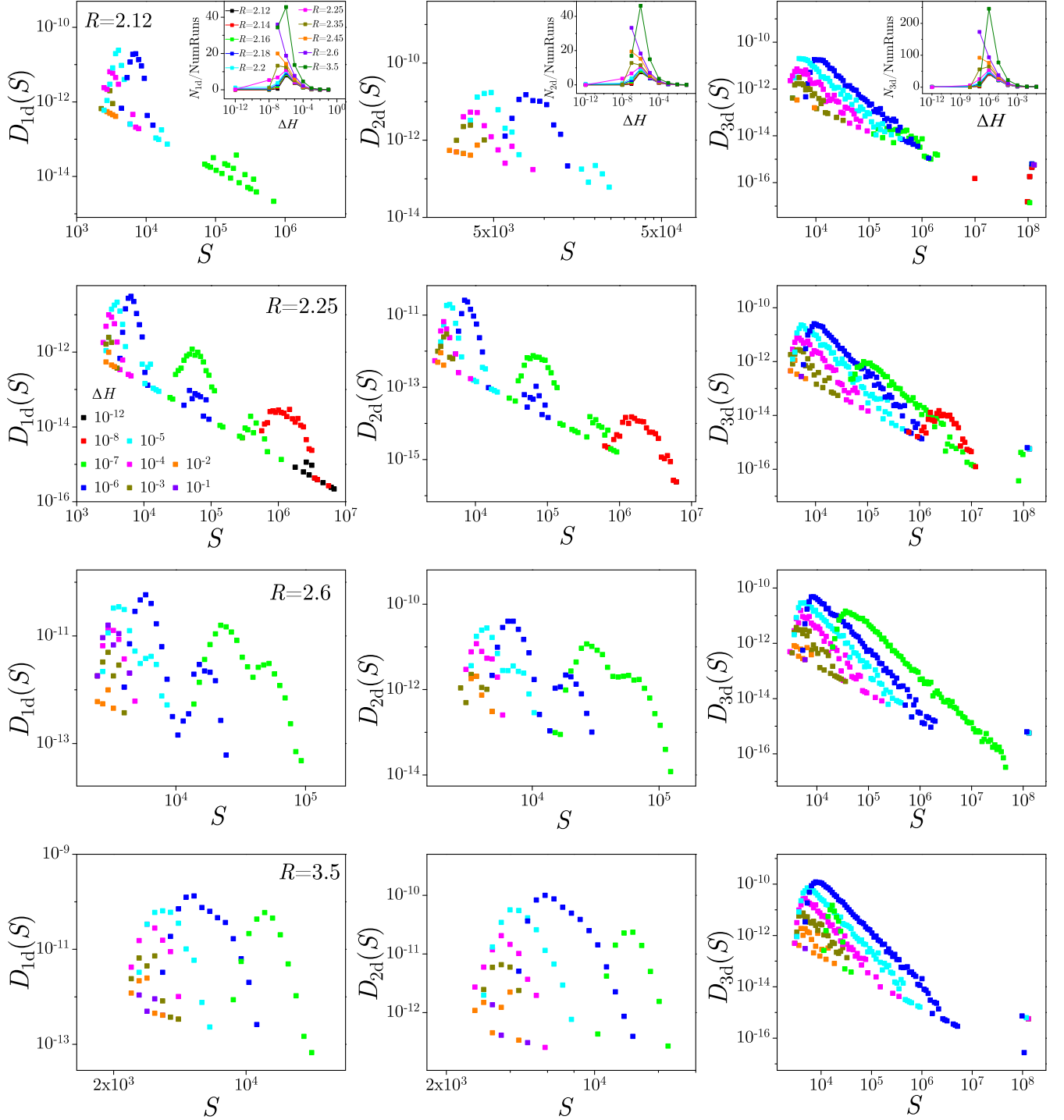


FIG. 9. Same as in Fig. 8 but for the systems driven with a finite driving rate.

quasistatic ones still remain without a plateau, whose occurrence is delayed and shown only in the range of fast driving rates, dominated by the rate-induced spanning avalanches. For high disorders and in slow driving, there appears a post-cutoff plateau previously found in [14]. Its level increases and eventually saturates at 1 merging with the main plateau due only to the rate-induced spanning, since the value of disorder prevents the creation of spanning avalanches. For fast driving rates, the shape of the correlation functions is determined and

dominated by the rate-induced spanning avalanches causing the plateau regardless of the system disorder.

D. Power spectra

Power spectrum $P(f)$ shows the mean power that is delivered at a frequency f by the response signal of the nonequilibrium model. In our study, it was estimated by implementation of the Welch method [47], which consists first

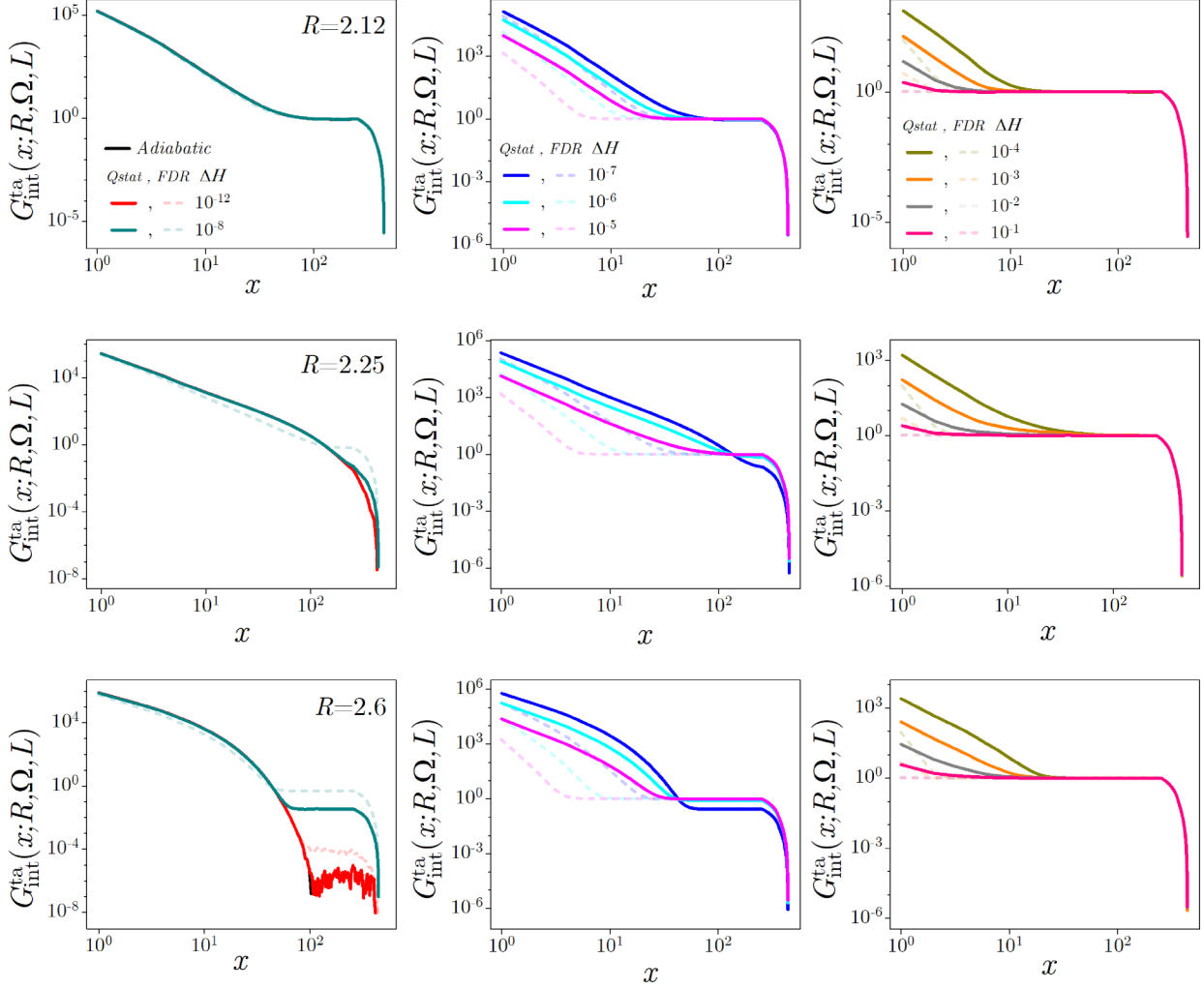


FIG. 10. Integrated triggered activity event correlation functions for disorders $R < R_c$, $R \geq R_c^{\text{eff}}$, and $R \gg R_c^{\text{eff}}$ (given in rows, respectively) in the slow, intermediate, and fast driving regimes (presented in columns) for all types of driving, calculated for the system with the same size $L = 512$ as in Fig. 2.

of multiplication of the response signal by the Welch window function, followed by an estimation of the power spectrum from the same length parts of the signal at the discrete frequencies. The resulting power spectrum $P(f)$ is obtained by averaging over the pertinent parts of all of the corresponding response signals obtained in the simulations. The power spectrum in each segment is calculated according to the following formula:

$$P_{\text{seg}}(f_n) = \frac{\Delta}{N} \left| \sum_k w_k V(t_k) e^{2\pi i f_n t_k} \right|^2, \quad (9)$$

where $f_n = n/(N\Delta)$; $n = 0, 1, \dots, N/2$ are the frequencies, Δ is the time step (here $\Delta = 1$), and N is the number of signal segments. w_k are the values of the window function, while t_k are the discrete moments of time at which the signal $V(t_k)$ is sampled. For more details, see [22,47,48]. RFIM studies performed so far showed that the power spectrum follows the power-law $P(f) \sim f^{-\gamma_{\text{ps}}}$ in a rather wide region of frequencies, named the scaling region, which is manifested as a linear portion of the $P(f)$ plot presented on a log-log scale. In Fig. 11 we show the power spectra for the quasistatic (top row panels)

and finite rate driving (bottom row panels) in three characteristic domains of disorder in a wide range of rates. We see that for the quasistatic driving, in the $R \leq R_c^{\text{eff}}$ disorder domain, the scaling region persists over a long range of frequencies, while for the fast driving the low-frequency spectra start to deviate from this form. In the finite-driven cases, the scaling region of spectra vanishes before the highest rates are even reached, showing a higher level of rate sensitivity in the power spectra of finite-driven systems. In [48] it was proposed that in the adiabatic regime of driving, the power-law exponent γ_{ps} of the power spectrum equals the exponent $\gamma_{S/T}$ describing the power-law $\langle S \rangle_T \sim T^{\gamma_{S/T}}$, where $\langle S \rangle_T$ is the mean size of avalanches having a duration T ; see Fig. 12. We check the validity of this proposition in the quasistatic and finite driving rate regimes by comparing independent estimates of the effective values of both exponents obtained by the linear fits of the scaling regions of the corresponding log-log plots. As can be seen in the insets of Fig. 12, both of the effective exponents $\gamma_{\text{ps}}^{\text{eff}}$ and $\gamma_{S/T}^{\text{eff}}$ show similar trends in their behavior as functions of ΔH in the case of driving with a finite rate, while in the case of quasistatic driving they practically overlap in the range of slow rates with emerging differences at increased rates.

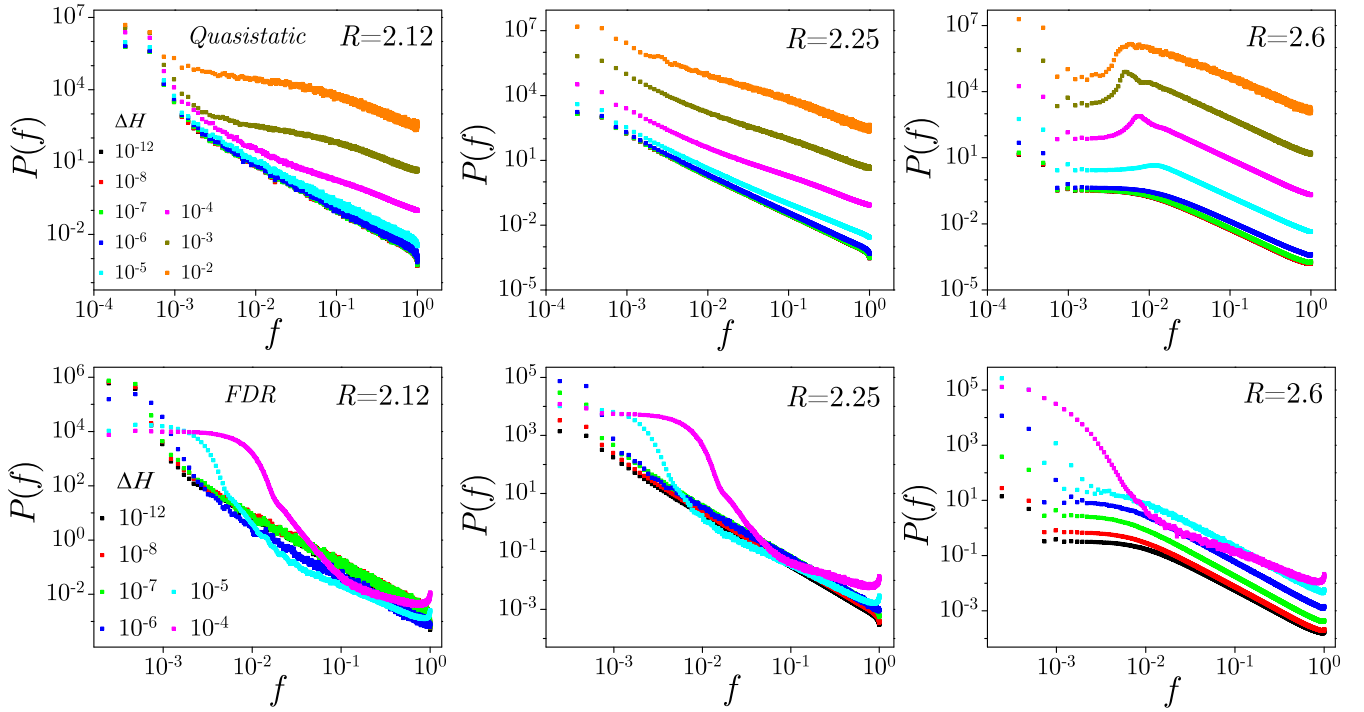


FIG. 11. Power spectra $P(f)$ for disorders $R < R_c$, $R \geq R_c^{\text{eff}}$, and $R \gg R_c^{\text{eff}}$ (presented in columns, respectively) in a wide range of driving rates for the quasistatic driving (top row) and for the driving with a finite rate (bottom row). The spectra pertain to the systems with the same size $L = 512$ as in Fig. 2.

Rate-dependent effective values of exponent $\gamma_{\text{ps}}^{\text{eff}}$, estimated in the power-law fitting of the scaling regions of power spectra, are presented in Fig. 13. These values are computed for the particular set of disorders representing the domains that are below, at, and above the effective critical disorder for the cases of quasistatic and finite-rate driving. In the case of quasistatic driving, presented in the left panel, we see that the values of the exponent remain fairly constant in the range of slow driving rates, followed by a decrease for the $R \leq R_c^{\text{eff}}$ case and an increase for the $R > R_c^{\text{eff}}$ case, respectively. On the other hand, for systems driven with a finite driving rate (right panel), we see similar trends in variation of γ_{eff} values with ΔH persisting regardless of the disorder of the system, i.e.,

approximately constant values in the region of slow rates, followed by a decrease with the increased rates.

IV. DISCUSSION AND CONCLUSION

The evolution of disordered nonequilibrium systems is affected by many factors. Isolating only one of them would not provide full insight into the underlying dynamics due to the intertwined nature and the complex influence they mutually impose. In this paper, we aimed to give a broader overlook of the interplay among the disorder, the driving rate, and the outcomes of the different ways in which external triggering is conducted while driving the system, i.e., the types of driving.

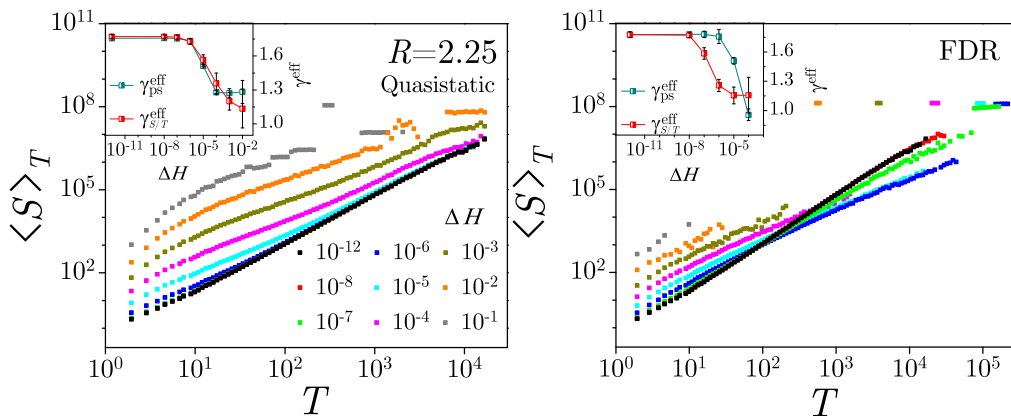


FIG. 12. Main panels: $\langle S \rangle_T$ for $R = R_c^{\text{eff}}$, for the quasistatic and finite-rate types of driving. The insets show the effective exponents $\gamma_{\text{ps}}^{\text{eff}}$ and $\gamma_{S/T}^{\text{eff}}$ vs ΔH estimated from the power-law fits of power spectra $P(f)$ and of the $\langle S \rangle_T$ plots, respectively, for the pertinent types of driving. Error bars are multiplied 10 times for better visibility.

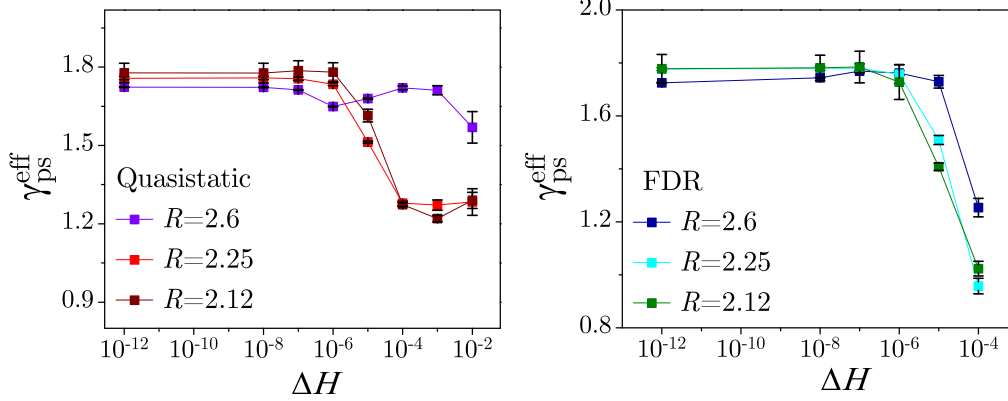


FIG. 13. Effective values of the rate-dependent exponent γ_{ps}^{eff} vs driving rate ΔH in the quasistatic (left panel) and finite-rate (right panel) regimes. The presented values are estimated from the power-law fits of scaling regions of the power spectra $P(f)$, shown in Fig. 11; the error bars are multiplied five times for better visibility.

The results of our study, obtained for disordered three-dimensional ferromagnetic systems by means of numerical simulations of the nonequilibrium athermal random field Ising model, reveal that the way the system is driven has an immense effect on its response. Our general remarks, based on analyses of magnetizations, distributions of avalanche parameters, correlation functions, and power spectra, are that as long as the driving of the external agent (here, the external magnetic field) is slow enough, the system's response can be approximated adiabatically. On the other hand, with an increase in the driving rate, starting from the intermediate regime of driving rates, the differences start to emerge. The reason for this is the occurrence of the simultaneous evolution of several avalanches developing at the shared or overlapped time interval, thus creating the overall system activity event that cannot be split into the contributions of particular avalanches, as is realized in the case of adiabatic driving. The onset of rate-induced multiflipping and merging into spanning avalanches occurs in the case of finite-rate driven systems for much slower rates than in the case of quasistatic driving, in which the increase in the magnetic field has to be several orders of magnitude bigger in order to achieve a similar effect.

The disparities due to the different types of driving are observed first in the output signal, starting from significant differences in the amplitudes shown in the fast regime, reducing with the decrease in the driving rate, and finally blending on top of another for all types of driving when the rates are slow enough. Analyzing the magnetizations and magnetic susceptibilities in the disorder domains $R \leq R_c^{\text{eff}}$ and in the slow rate regime, we find practically no difference for all types of driving. With the increase in the rate, the differences start to show, most prominently in the fast driving regime. When $R > R_c^{\text{eff}}$, intermediate regime magnetizations fuse with slow ones, ultimately reaching rate independence for $R \gg R_c^{\text{eff}}$ in the quasistatically driven systems, while for fast driving the differences persist even for very high disorders. Estimated values of effective critical magnetic field H_c^{eff} turn out to be rate-dependent as well, and their flow with the rate qualitatively resembles the flow of a coercive field calculated from experimental data obtained on thin films [41].

Similar conclusions emerge from the analysis of avalanche distributions. We studied both the integrated distributions comprising all types of avalanches, and also the integrated distributions of each type individually. We find that, regardless of the disorder, integrated size distributions in the slow driving regime approximately overlap for all types of driving. Differences between the distributions start to show with the increase of both the disorder and the driving rate in the quasistatically and finite-rate driven systems, being most prominent in the fast driving regime due to the intensified merging and overlapping of simultaneously propagating avalanches. The onset of rate-attributed spanning avalanches can be seen in the typical bumps preceding the cutoff of the distributions, which also affects the value of the slope of the distributions, consequently altering the values of the pertinent effective exponents, making them rate-dependent. The flow of the exponents with the driving rate is in accordance with that found in [30]. Nonspanning avalanche size distributions, qualitatively speaking, have similar trends, with the difference in the characteristic dents at the ends of distributions marking the onset of rate-induced spanning avalanches that are removed from this type of distribution. Distributions of 1D and 2D spanning avalanches clearly demonstrate the double source of their origin. Namely, for slow drivings and low disorders, these distributions have a single peak due to the solely disorder-induced spanning avalanches. With the increase in the driving rate, the second peak appears. With a further increase in the rate, this second peak starts to merge with the first one, resulting in a transitional double-peaked distribution. This leads eventually to a single peak again for big values of disorders and fast driving rates, denoting the single, in this case rate-attributed, origin. On the other hand, 3D spanning avalanches remain power-law-distributed over all domains of disorder and ranges of driving rates.

Regarding the correlation functions, the variation of disorder (along with the rate value and type of driving) has similar effects to those previously described. Dominated by the disorder-induced spanning avalanches in the low disorder domain and for all driving regimes, the integrated triggered activity event correlation functions are marked with the characteristic plateau. With the increase of disorder close to the effective critical value and for small driving rates, the plateau

disappears as well as the spanning types of avalanches, causing the correlation functions to have a typical adiabatic-like decrease with the distance among the correlated spins. With a further increase of disorder, while still remaining in the range of slow driving rates, a new plateau starts to form in the area after the cutoff, but at heights much below the main plateau saturating at 1. This effect was previously observed in [14], with the levels of these plateaus increasing with the driving rate, finally reaching and overlapping with the main plateau and saturating at 1. In the fast driving regime, the main plateau persists supported by the rate-attributed spanning avalanches present in the system.

Power spectra for the quasistatically driven systems in the domains of low and intermediate disorder preserve a stable power-law trend persisting over several decades of scaling. A similar trend applies to the high-frequency part in the fast driving regime, while for the low-frequency portions, power spectra start to deviate. The rate affects power spectra much more in the case of finite-rate driving, destroying the power-law part even for lower values of driving rates. Effective values of the exponent γ^{eff} estimated from the power spectrum and the mean size of avalanches with a fixed duration show similar trends with the driving rates in the case of quasistatic driving, in which they are almost overlapping, while for finite driving these flows look fairly similar in a qualitative sense.

To conclude, in this paper we have investigated the effects of adiabatic, quasistatic, and finite-rate types of driving on the evolution of the systems, described by means of the nonequilibrium athermal random field Ising model. The effects were studied in all three domains of disorder (low, high, and transitional) for all types of driving, and in a wide range of driving rates for quasistatic and finite-rate types of driving. We found that as long as the driving is slow enough, such systems behave as effectively being driven adiabatically, while with an increase in the driving rate the departure from adiabatic behavior is more and more apparent as the rate increases. In the domain of low disorder, disorder-induced spanning avalanches dominate regardless of the type of driving. In the high disorder domain, however, only for the fast driving rates does the second origin of the spanning avalanches emerge, namely the rate-induced spanning. According to our results, the described behavior is demonstrated for the magnetizations, avalanche parameters distributions, correlation functions, and power spectra.

We hope that our results will bring some new understanding and could be of relevance for future research on a variety of systems undergoing a similar type of evolution in response to external driving. This is particularly applicable to cases in which the phenomena of interest are so complex that they cannot be realized experimentally.

ACKNOWLEDGMENTS

We acknowledge the support by the Ministry of Education, Science and Technological Development of Republic of Serbia (Agreements No. 451-03-68/2022-14/200162 and No. 451-03-68/2022-14/200122).

APPENDIX A: ON THE EFFECT OF DIFFERENT CHOICE OF THE RANDOM FIELD DISTRIBUTION

The influence that the functional form of the random-field distribution has on the adiabatic system's response was the subject of some previous studies. For example, in Ref. [32], it was studied in the case of equilateral (3D) cubic systems using four different types of distributions: (i) Gaussian, $f_G(h) = \exp(-h^2/2R^2)/R\sqrt{2\pi}$; (ii) Lorentzian, $f_L(h) = R/2\pi[h^2 + (R/2)^2]$; (iii) parabolic, $f_P(h) = 3(R^2 - h^2)/4R^3$ for $h \in [-R, R]$ and 0 elsewhere; and (iv) uniform, $f_U(h) = 1/2R$ for $h \in [-R, R]$ and 0 elsewhere. It was demonstrated that, except for the uniform distribution, the other three distributions, all unimodal, lead to the same values of critical exponents and scaling functions, implying the shared universality class to which they belong.

Our preliminary results, obtained (like in [32]) for $L = 64$ and shown in Figs. 14 and 15, suggest that this might also be the case for the double-Gaussian distribution. Its version, studied in [49], reads

$$f_{\text{DG}}(h) = \frac{1}{2} \left[\frac{e^{-(h-\delta H)^2/2\sigma_{\text{DG}}^2}}{\sigma_{\text{DG}}\sqrt{2\pi}} + \frac{e^{-(h+\delta H)^2/2\sigma_{\text{DG}}^2}}{\sigma_{\text{DG}}\sqrt{2\pi}} \right], \quad (\text{A1})$$

and it is comprised of two Gaussians (2) centered at $-\delta H$ and $+\delta H$, both with standard deviation σ_{DG} , in which case $R = \sqrt{\sigma_{\text{DG}}^2 + \delta H^2}$ is the standard deviation of double-Gaussian version (A1).

Thus, the data shown in Fig. 14 suggest that the integrated size distributions $D(S)$, multiplied by $S^{\tau'}$, can be collapsed according to

$$D(S) = \mathcal{D}(rS^{\sigma'})/S^{\tau'}, \quad (\text{A2})$$

onto a scaling function $\mathcal{D}(rS^{\sigma'})$ of a single argument $rS^{\sigma'}$. More specifically, the data from the left panel of Fig. 14 confirm this in the adiabatic case for all of the aforementioned distributions of random field (except uniform), and additionally suggest that this might also be the case for the quasistatic and finite-rate driving provided that the driving speed is not too high. At higher speed, the data shown in the other two panels of Fig. 14 indicate that the collapsing (A2) might still be achievable, but at the cost of different forms of scaling function $\mathcal{D}(rS^{\sigma'})$ and using different (i.e., effective) values of exponents τ' and σ' ; note, however, that for data from the left panel, the collapsing is achieved using the (standard) adiabatic values $\tau' = 2.03 (= \tau + \sigma\beta\delta)$ and $\sigma' = 0.24 (= \sigma)$ of these exponents, quoted in, e.g., Ref. [8].

The foregoing findings are further supported by the data from Fig. 15, showing the susceptibility curves collapsed according to

$$r^{(\beta\delta)' - \beta'} \chi(H) = \tilde{\chi} \left(\frac{H - H_c^{\text{eff}}(R)}{r^{(\beta\delta)'}} \right) \quad (\text{A3})$$

using effective exponents $(\beta\delta)'$ and β' . Except for fast driving, the collapsing seems to be achievable using the adiabatic values of these two exponents, $(\beta\delta)' = 2$ and $\beta' = 0.04$; see Ref. [17]. On the other hand, for fast driving in the finite-rate regime, the collapsing still seems to be possible for each individual distribution, but for different distribution-specific values of the effective exponents $(\beta\delta)'$ and β' . Being obtained

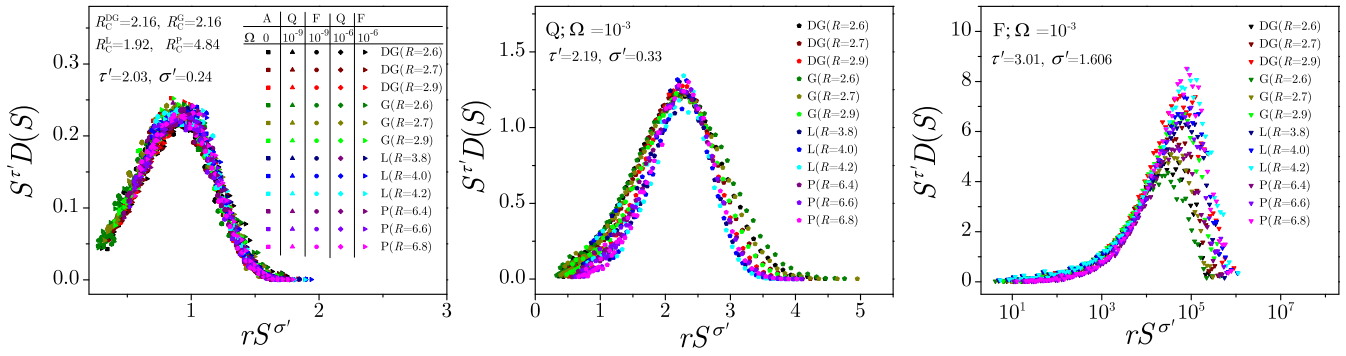


FIG. 14. Scaling collapse (A2) of the integrated distribution $D(S)$ of activity event size S for double-Gaussian (DG), Gaussian (G), Lorentzian (L), and parabolic (P) distributions of random fields. The left panel shows the data obtained in adiabatic (A), quasistatic (Q), and finite-rate (F) driving regimes for the values of driving speed Ω and the distribution-specific values of disorder parameter R shown in the legend; for double-Gaussian distributions, we used a minimum value of $\delta H = \sigma_{DG} = R/\sqrt{2}$ required for a clean separation of the Gaussians. The collapsing is achieved independently for each type of random field distribution using reduced disorder $r = (R - R_c)/R$, and adiabatic values 2.03 and 0.24 for the exponents τ' and σ' quoted in [8] as $\tau + \sigma\beta\delta$ and σ . The collapses obtained in this way span different ranges along both axes and are therefore, as in Ref. [32], additionally scaled by distribution-dependent scale factors so as to overlap with data corresponding to the Gaussian distribution. Analogous collapses for fast driving in quasistatic and finite-rate regimes are shown in the middle and right panels, respectively. For computational convenience and easier comparison with the results presented in Ref. [32], all simulations are performed on relatively small systems of size $L = 64$ with a number of runs up to 10 000 for a single set of simulation parameters.

on relatively small systems, these and the foregoing findings should be systematically tested on larger systems, which could be the subject of a separate future study.

APPENDIX B: SIZE EFFECTS FOR THE CASE OF QUASISTATIC DRIVING

Finite-size effects in the cases of adiabatic and finite-rate driving have already been studied previously (see [17] and [30] for more details). Here we supplement these findings by considering the size effects for the case of quasistatic driving. In Fig. 16 we show the magnetizations and susceptibilities for different system sizes ($L = 256, 512, 1024$), presented for three different disorders ($R = 2.6, 3.0, 4.0$) and for values of field increments chosen to be representative of slow ($\Delta H = 10^{-9}$), intermediate ($\Delta H = 10^{-6}$), and fast ($\Delta H = 10^{-3}$) driving cases. As can be seen, all data for the same set of

parameters and various size L practically overlap, indicating that the magnetization and pertaining susceptibilities of the system for high disorders become size-independent regardless of the considered driving regime. This further justifies our choice of $L = 512$ as a representative system size for our study.

APPENDIX C: THE EFFECTIVE CRITICAL PARAMETERS $R_c^{\text{eff}}(L)$, $\Omega_c^{\text{eff}}(R, L)$, $\Omega_c(R)$, and $H_c^{\text{eff}}(R, L)$

For magnetic systems in the thermodynamic limit, the phase transition is manifested by a jump in magnetization, which in the case of *adiabatically* driven NE-ZT-RFIM spin systems is caused by an infinite avalanche that appears in infinite systems only at disorders below the critical disorder R_c . In the *finite* spin systems of this kind, the role of infinite avalanches is played by the spanning avalanches, which are

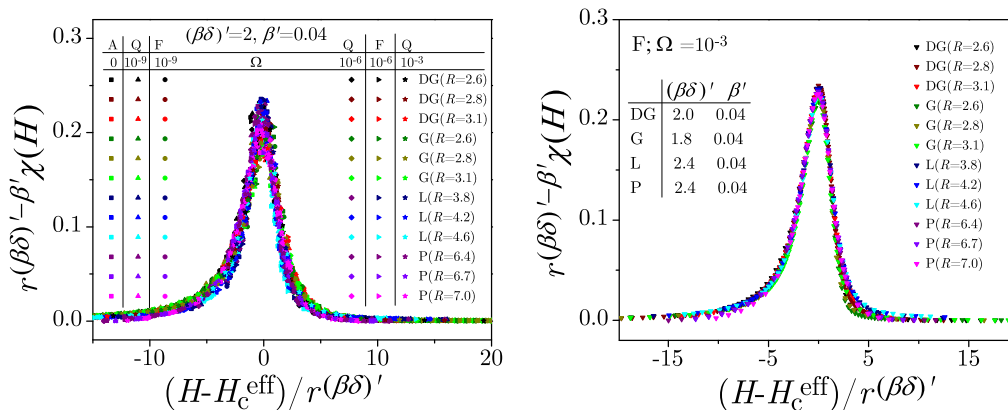


FIG. 15. Scaling collapse (A3) of the susceptibility curves $\chi(H)$ obtained in the same set of simulations as for the data shown in Fig. 14. In the left panel we used adiabatic values 2 and 0.04 for the exponents $(\beta\delta)'$ and β' quoted in Ref. [17] as $\beta\delta$ and β , while the collapsing from the right panel, corresponding to the fast finite-rate driving, is achieved using distribution-specific values of these exponents quoted in the legend. For the collapsing curves, H_c^{eff} is the abscissa of the maximum on this curve, and is separately determined for each of them.

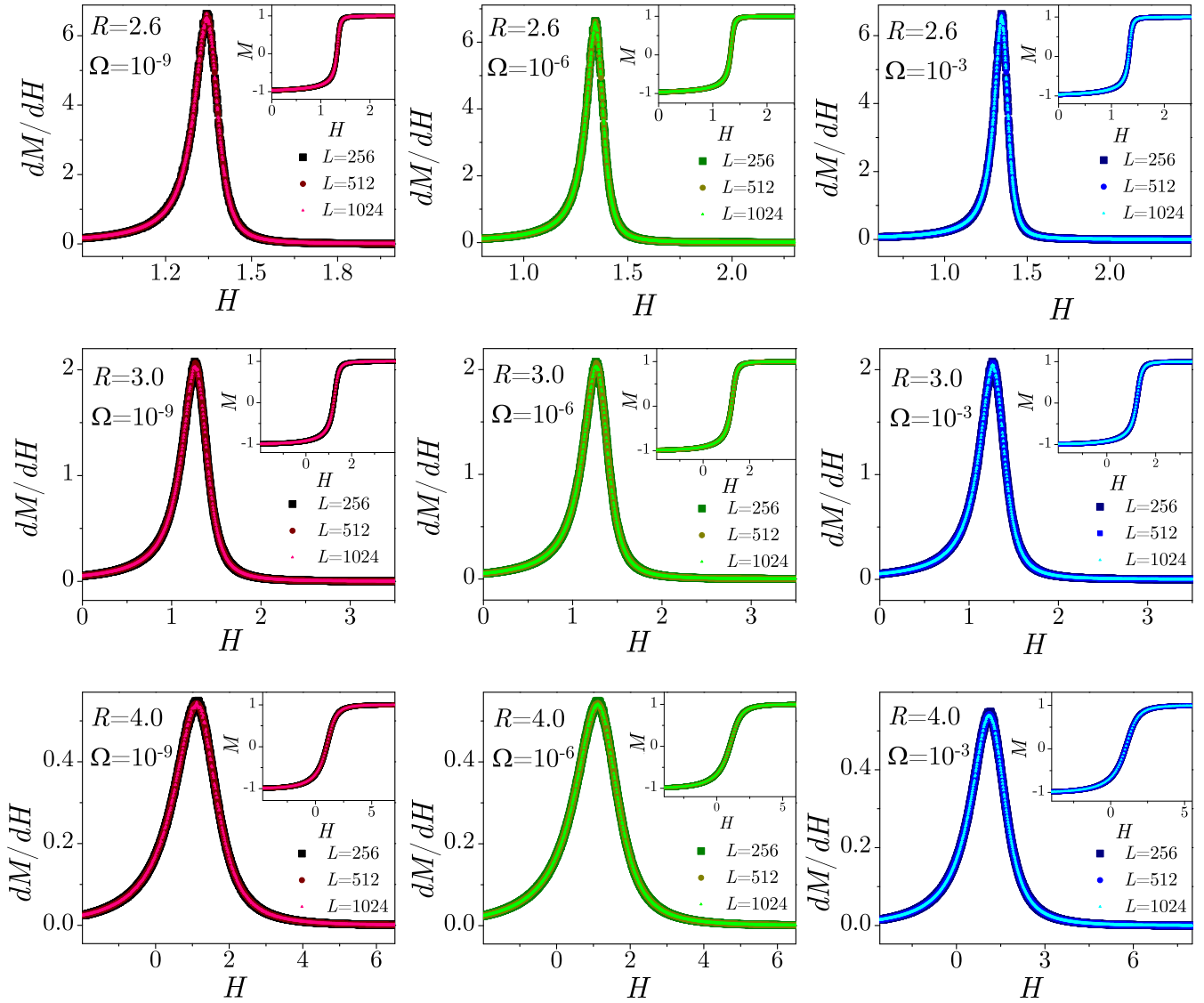


FIG. 16. Susceptibilities (main panels) and magnetizations (insets) obtained for quasistatically driven systems, whose size, disorder, and field increments are shown in the legends. Data are averaged over up to 50 different realizations of random magnetic field.

likely/unlikely to appear at disorders that are below/above a size-dependent effective critical disorder $R_c^{\text{eff}} > R_c$, as is shown in [17] for the systems situated at the equilateral cubic lattices of (finite) size L . There, the value $R_c^{\text{eff}}(L)$ of effective critical disorder separates the domain of *high*, $R > R_c^{\text{eff}}(L)$, from a narrow domain of *transitional*, $R_c < R < R_c^{\text{eff}}(L)$, disorders vanishing when $L \rightarrow \infty$ and continued by the domain of *low* disorders $R < R_c$; see Appendix D.

In the quasistatic and finite-rate driving regimes, the activity events (i.e., the set of simultaneously propagating avalanches) that span the system appear as well at low disorders $R < R_c^{\text{eff}}(L)$ regardless of the driving speed because the low enough disorder is already sufficient for their onset. On the other hand, the activity events in these two regimes, aided by the finite increments ΔH to become spanning, also appear at disorders $R > R_c^{\text{eff}}(L)$ provided that the system is driven fast enough. This means that for any value of disorder $R > R_c^{\text{eff}}(L)$ there is an effective critical driving speed $\Omega_c^{\text{eff}}(R, L)$ such that

the spanning activity events are absent/present below/above it in the systems of size L . The values of $\Omega_c^{\text{eff}}(R, L)$ for the quasistatic driving are different from the corresponding values for finite-rate driving, discussed in [30]. The values for both types of driving are depicted by symbols in the upper panel of Fig. 17, whereas full lines show the values of critical driving speed $\Omega_c^{\text{eff}}(R)$, estimated as limits $\Omega_c(R) = \lim_{L \rightarrow \infty} \Omega_c^{\text{eff}}(R, L)$. Each of these two lines is the boundary between the region of *slow*, i.e., $\Omega < \Omega_c(R)$, and *fast*, i.e., $\Omega > \Omega_c(R)$, driving for the corresponding driving regime of infinite systems, whereas for finite systems, *intermediate*, i.e., $\Omega_c(R) < \Omega < \Omega_c^{\text{eff}}(R, L)$, rates separate slow from fast driving, $\Omega > \Omega_c^{\text{eff}}(R, L)$. The values of $\Omega_c(R)$ increase with R , and the flow for quasistatic driving qualitatively resembles that for finite-rate driving, but the values belong to the range of higher rates.

Besides the critical driving speed, in the bottom panel of Fig. 17 we show against disorder R the flow of the effective

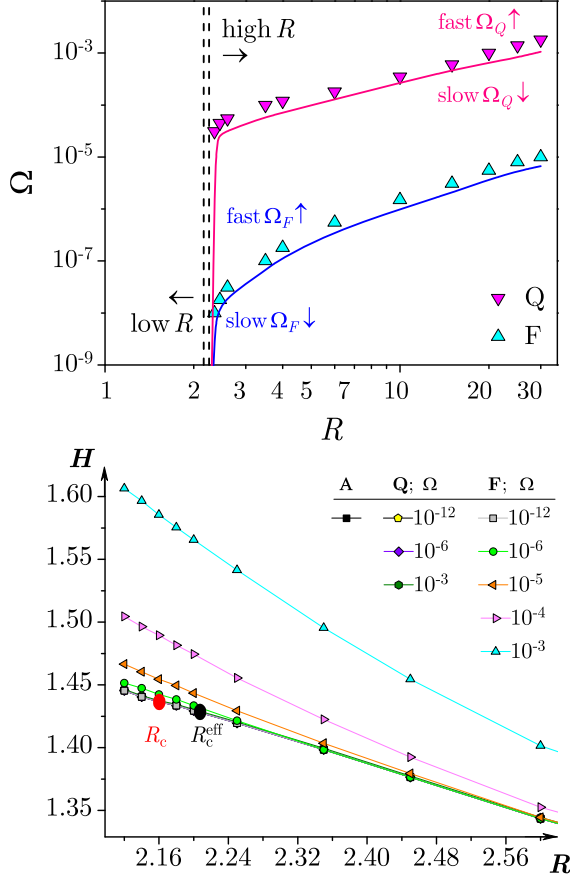


FIG. 17. Top panel: phase diagram showing the effective critical driving rate Ω_c^{eff} against disorder R in the quasistatic (Q) and finite-rate (F) regimes. Two vertical dashed lines bound the (narrow) region of transitional disorders for $L = 512$. Bottom panel: the effective critical magnetic field $H_c^{\text{eff}}(R, L)$ vs disorder R in adiabatic (A), quasistatic (Q), and finite-rate (F) regimes, the latter two for the values of driving rate Ω shown in the legend. Symbols show the data $\Omega_c^{\text{eff}}(R, L)$ and $H_c^{\text{eff}}(R, L)$ for the system size $L = 512$, averaged over up to 50 different realizations of random magnetic field. The full lines in the top panel depict the estimated values of the critical driving speed $\Omega_c(R) = \lim_{L \rightarrow \infty} \Omega_c^{\text{eff}}(R, L)$, while in bottom panel they connect the symbols for better visibility.

critical magnetic field $H_c^{\text{eff}}(R, L)$, estimated from the corresponding susceptibility maxima. Presented data are obtained for all three types of driving (adiabatic, quasistatic, and finite-rate), as is shown in the legend. Provided the spanning activity events are present, the jump (more precisely, the sharp increase) in magnetization occurs at this value of the external magnetic field. One can see the overlapping of the values obtained for adiabatic and for slow quasistatic and finite-rate

driving, which is in accordance with the rest of our findings presented in this paper. With the increase in driving rate, the flow is systematically shifted vertically to higher magnetic field values.

APPENDIX D: ON THE METHOD FOR ESTIMATION OF THE EFFECTIVE CRITICAL DISORDER $R_c^{\text{eff}}(L)$

In this Appendix, we briefly outline the method used for the estimation of the effective critical disorder $R_c^{\text{eff}}(L)$ in Ref. [17].

In 3D spins systems, situated at finite equilateral cubic lattices and described by the adiabatically driven NE-ZT-RFIM with Gaussian distribution of random fields, the spanning avalanches are classified according to the number of spatial dimensions they span as 1D, 2D, and 3D spanning avalanches. The average number of spanning avalanches per single run depends on disorder R , lattice size L , and the type of spanning avalanche. This number for the 1D spanning avalanches and lattice size L , taken as a function of disorder R , forms a distribution $N_{1D}(R; L)$ along the R -axis showing by its nonzero values the likelihood for the 1D spanning avalanche to appear at the corresponding disorder R .

The distribution $N_{1D}(R; L)$ is unimodal and well described by a Gaussian. Its mode, showing the value of disorder at which the 1D spanning avalanches are most probable, is taken as the effective critical disorder estimated by the 1D spanning avalanches at the current L , while its standard deviation, quantifying the width of the region of disorder values in which the 1D spanning avalanches are likely, is taken as the range of transitional disorder. When $L \rightarrow \infty$, the standard deviation tends to zero, while the mode tends to some limit which is taken as the value of critical disorder estimated by the 1D spanning avalanches. The distribution $N_{2D}(R; L)$ for 2D spanning avalanches behaves in an analogous way.

On the other hand, the distributions $N_{3D}(R; L)$ of 3D spanning avalanches have a more complex form which was found to be well described by a superposition of complementary error function and a Gaussian centered near the inflection point of (transitional region of) the complementary error function having approximately the same width of the transitional region as the superposed Gaussian. Therefore, the quantities in question are taken as the effective critical disorder, and the width of the domain of transitional disorders is estimated by the 3D spanning avalanches. The distribution $N_s(R; L)$ for all spanning avalanches behaves analogously.

Although not exactly the same, all the foregoing estimates agree within their error bars enabling definition of the effective critical disorder and the range of transitional disorders whose upper boundary is not sharp, as is the case for any

TABLE I. Values of the effective critical disorder $R_c^{\text{eff}}(L)$ and of the effective critical field $H_c^{\text{eff}}(L)$ for the adiabatically driven system of size L having Gaussian distribution of the random magnetic field.

L	128	180	256	360	512	724	1024	1448	2048
$R_c^{\text{eff}}(L)$	2.282	2.256	2.234	2.217	2.205	2.194	2.187	2.181	2.177
$H_c^{\text{eff}}(L)$	1.413	1.419	1.422	1.426	1.428	1.429	1.432	1.433	1.434

other quantity of statistical kind, while its lower boundary is taken by convention at critical disorder R_c .

Finally, for system sizes in the range $L = 128$ – 2048 we present in Table I the values of effective critical disorder $R_c^{\text{eff}}(L)$ estimated from the average numbers of spanning

avalanches per single run, and also the estimated values of the effective critical field $H_c^{\text{eff}}(L)$, i.e., the value of external magnetic field at which the susceptibility curve, obtained in the adiabatic regime at disorder $R = R_c^{\text{eff}}(L)$, has its maximum. For more details, see Ref. [17].

-
- [1] D. S. Fisher, Collective transport in random media: from superconductors to earthquakes, *Phys. Rep.* **301**, 113 (1998).
- [2] J. Davidsen and M. Baiesi, Self-similar aftershock rates, *Phys. Rev. E* **94**, 022314 (2016).
- [3] O. A. Pinto and M. A. Muñoz, Quasi-neutral theory of epidemic outbreaks, *PLoS ONE* **6**, e21946 (2011).
- [4] J. P. Bouchaud, Crises and collective socio-economic phenomena: Simple models and challenges, *J. Stat. Phys.* **151**, 567 (2013).
- [5] A. Bizzarri, A. Petri, and A. Baldassarri, Earthquake dynamics constrained from laboratory experiments: new insights from granular materials, *Ann. Geophys.* **64**, 441 (2021).
- [6] P. D. Ispánovity *et al.*, Dislocation avalanches are like earthquakes on the micron scale, *Nat. Commun.* **13**, 1975 (2022).
- [7] D. P. Belanger and T. Nattermann, in *Spin Glasses and Random Fields*, edited by A. P. Young (World Scientific, Singapore, 1998), pp. 251–298.
- [8] J. P. Sethna, K. A. Dahmen, and O. Perković, Random-field Ising models of hysteresis, in *The Science of Hysteresis*, edited by G. Bertotti and I. Mayergoyz (Academic, Amsterdam, 2006), Vol. 2, pp. 107–179.
- [9] D. Spasojević, S. Bukvić, S. Milošević, and H. E. Stanley, Barkhausen noise: Elementary signals, power laws, and scaling relations, *Phys. Rev. E* **54**, 2531 (1996).
- [10] A. Skaugen and L. Laurson, Depinning Exponents of Thin Film Domain Walls Depend on Disorder Strength, *Phys. Rev. Lett.* **128**, 097202 (2022).
- [11] N. Friedman, S. Ito, B. A. W. Brinkman, M. Shimon, R. E. L. DeVill, K. A. Dahmen, J. M. Beggs, and T. C. Butler, Universal Critical Dynamics in High Resolution Neuronal Avalanche Data, *Phys. Rev. Lett.* **108**, 208102 (2012).
- [12] S. R. Miller, S. Yu, and D. Plenz, The scale-invariant, temporal profile of neuronal avalanches in relation to cortical γ -oscillations, *Sci. Rep.* **9**, 16403 (2019); see also *Criticality in Neural Systems*, edited by D. Plenz and E. Niebur (Wiley Online Library, 2014).
- [13] J. T. Uhl *et al.*, Universal quake statistics: From compressed nanocrystals to earthquakes, *Sci. Rep.* **5**, 16493 (2015).
- [14] D. Spasojević, S. Radić, D. Jovković, and S. Janićević, Spin activity correlations in driven disordered systems, *J. Stat. Mech.* (2022) 063302.
- [15] J. P. Sethna, K. A. Dahmen, S. Kartha, J. A. Krumhansl, B. W. Roberts, and J. D. Shore, Hysteresis and Hierarchies: Dynamics of Disorder-Driven First-Order Phase Transformations, *Phys. Rev. Lett.* **70**, 3347 (1993).
- [16] O. Perković, K. A. Dahmen, and J. P. Sethna, Disorder-induced critical phenomena in hysteresis: Numerical scaling in three and higher dimensions, *Phys. Rev. B* **59**, 6106 (1999).
- [17] S. Janićević, D. Knežević, S. Mijatović, and D. Spasojević, Scaling domains in the nonequilibrium athermal random field Ising model of finite systems, *J. Stat. Mech.* (2021) 013202.
- [18] S. Graovac, S. Mijatović, and D. Spasojević, Mechanism of subcritical avalanche propagation in three-dimensional disordered systems, *Phys. Rev. E* **103**, 062123 (2021).
- [19] D. Spasojević, S. Janićević, and M. Knežević, Numerical Evidence for Critical Behavior of the Two-Dimensional Nonequilibrium Zero-Temperature Random Field Ising Model, *Phys. Rev. Lett.* **106**, 175701 (2011).
- [20] D. Spasojević, S. Janićević, and M. Knežević, Avalanche distributions in the two-dimensional nonequilibrium zero-temperature random field Ising model, *Phys. Rev. E* **84**, 051119 (2011).
- [21] D. Spasojević, S. Mijatović, V. Navas-Portela, and E. Vives, Crossover from three-dimensional to two-dimensional systems in the nonequilibrium zero-temperature random-field Ising model, *Phys. Rev. E* **97**, 012109 (2018).
- [22] S. Janićević, S. Mijatović, and D. Spasojević, Critical behavior of the two-dimensional nonequilibrium zero-temperature random field Ising model on a triangular lattice, *Phys. Rev. E* **95**, 042131 (2017).
- [23] S. Mijatović, D. Jovković, and D. Spasojević, Nonequilibrium athermal random-field Ising model on hexagonal lattices, *Phys. Rev. E* **103**, 032147 (2021).
- [24] B. Tadić, S. Mijatović, S. Janićević, D. Spasojević, and G. J. Rodgers, The critical Barkhausen avalanches in thin random-field ferromagnets with an open boundary, *Sci. Rep.* **9**, 6340 (2019).
- [25] S. Mijatović, D. Jovković, S. Janićević, and D. Spasojević, Critical disorder and critical magnetic field of the nonequilibrium athermal random-field Ising model in thin systems, *Phys. Rev. E* **100**, 032113 (2019).
- [26] S. Mijatović, M. Branković, S. Graovac, and D. Spasojević, Avalanche properties in striplike ferromagnetic systems, *Phys. Rev. E* **102**, 022124 (2020).
- [27] B. Tadić, Dynamic criticality in driven disordered systems: role of depinning and driving rate in Barkhausen noise, *Physica A* **270**, 125 (1999).
- [28] S. L. A. de Queiroz and M. Bahiana, Finite driving rates in interface models of Barkhausen noise, *Phys. Rev. E* **64**, 066127 (2001).
- [29] R. A. White and K. A. Dahmen, Driving Rate Effects on Crackling Noise, *Phys. Rev. Lett.* **91**, 085702 (2003).
- [30] S. Radić, S. Janićević, D. Jovković, and D. Spasojević, The effect of finite driving rate on avalanche distributions, *J. Stat. Mech.* (2021) 093301.
- [31] D. Spasojević and S. Janićević, Two-dimensional ferromagnetic systems with finite driving, *Chaos, Solitons Fractals* **158**, 112033 (2022).
- [32] Y. Liu and K. A. Dahmen, Unexpected universality in static and dynamic avalanches, *Phys. Rev. E* **79**, 061124 (2009).

- [33] I. Balog, G. Tarjus, and M. Tissier, Criticality of the random field Ising model in and out of equilibrium: A nonperturbative functional renormalization group description, *Phys. Rev. B* **97**, 094204 (2018).
- [34] N. G. Fytas, V. Martin-Mayor, M. Picco, and N. Surlas, Phase Transitions in Disordered Systems: The Example of the Random-Field Ising Model in Four Dimensions, *Phys. Rev. Lett.* **116**, 227201 (2016).
- [35] N. G. Fytas, V. Martin-Mayor, G. Parisi, M. Picco, and N. Surlas, Evidence for Supersymmetry in the Random-field Ising Model at $d = 5$, *Phys. Rev. Lett.* **122**, 240603 (2019).
- [36] G. Parisi and N. Surlas, Random Magnetic Fields, Supersymmetry, and Negative Dimensions, *Phys. Rev. Lett.* **43**, 744 (1979).
- [37] J. Bricmont and A. Kupiainen, Lower Critical Dimension for the Random-field Ising Model, *Phys. Rev. Lett.* **59**, 1829 (1987).
- [38] G. Parisi and N. Surlas, Scale Invariance in Disordered Systems: The Example of the Random-Field Ising Model, *Phys. Rev. Lett.* **89**, 257204 (2002).
- [39] M. Tissier and G. Tarjus, Supersymmetry and Its Spontaneous Breaking in the Random Field Ising Model, *Phys. Rev. Lett.* **107**, 041601 (2011).
- [40] M. Kuntz, O. Perković, K. A. Dahmen, B. W. Roberts, and J. P. Sethna, Hysteresis, avalanches, and noise, *Comput. Sci. Eng.* **1**, 73 (1999).
- [41] T. A. Moore, J. Rothman, Y. B. Xu, and J. A. C. Bland, Thickness-dependent dynamic hysteresis scaling behavior in epitaxial Fe/GaAs(001) and Fe/InAs(001) ultrathin films, *J. Appl. Phys.* **89**, 7018 (2001).
- [42] D. Spasojević, S. Janičević, and M. Knežević, Analysis of spanning avalanches in the two-dimensional nonequilibrium zero-temperature random-field Ising model, *Phys. Rev. E* **89**, 012118 (2014).
- [43] F. J. Pérez-Reche and E. Vives, Finite-size scaling analysis of the avalanches in the three-dimensional Gaussian random-field Ising model with metastable dynamics, *Phys. Rev. B* **67**, 134421 (2003).
- [44] F. J. Pérez-Reche and E. Vives, Spanning avalanches in the three-dimensional Gaussian random-field Ising model with metastable dynamics: Field dependence and geometrical properties, *Phys. Rev. B* **70**, 214422 (2004).
- [45] A. Rosso, P. Le Doussal, and K. J. Wiese, Avalanche-size distribution at the depinning transition: A numerical test of the theory, *Phys. Rev. B* **80**, 144204 (2009).
- [46] K. A. Dahmen and J. P. Sethna, Hysteresis, avalanches, and disorder induced critical scaling: A renormalization group approach, *Phys. Rev. B* **53**, 14872 (1996).
- [47] W. H. Press, S. A. Teukolsky, W. T. Vetterling, and B. P. Flannery, *Numerical Recipes: The Art of Scientific Computing*, 3rd ed. (Cambridge University Press, Cambridge, 2007).
- [48] M. C. Kuntz and J. P. Sethna, Noise in disordered systems: The power spectrum and dynamic exponents in avalanche models, *Phys. Rev. B* **62**, 11699 (2000).
- [49] G. Karakoyun and U. Akinci, Effects of the double Gaussian random field distribution on the phase diagrams and hysteresis characteristics of the magnetic binary alloys, *J. Phys. B* **578**, 411870 (2020).